PACIFIC EARTHQUAKE ENGINEERING
RESEARCH CENTER

Retest of Thirty-Year-Old Neoprene Isolation Bearings

James M. Kelly
Department of Civil and Environmental Engineering
University of California, Berkeley

Niel C. Van Engelen
Department of Civil Engineering
McMaster University

PEER 2014/03
MARCH 2014

Retest of Thirty-Year-Old Neoprene Isolation Bearings

James M. Kelly
Department of Civil and Environmental Engineering
University of California, Berkeley

Niel C. Van Engelen
Department of Civil Engineering
McMaster University

PEER Report 2014/03
Pacific Earthquake Engineering Research Center
Headquarters at the University of California, Berkeley

March 2014

ABSTRACT

A set of Neoprene isolation bearings remaining from a 1981 shake table test series conducted at the Earthquake Simulator Laboratory at the Earthquake Engineering Research Center (now the Pacific Earthquake Engineering Research Center) were retested in 2012. The new test series was conducted at the NEES site at the Richmond Field Station, University of California, Berkeley. The retest program had the dual purpose of determining the changes in the isolation properties, namely, the horizontal stiffness and equivalent viscous damping, and to study the behavior of the isolators at dynamic inputs that constitute beyond design-basis earthquake levels.

Two types of isolators were considered in the 1981 test series: the first made with a stiff compound (50 durometer), and the second made with a much softer compound (40 durometer). The 2012 study investigated a total of six isolators, three of each compound. The experimental testing revealed that a significant increase in horizontal stiffness and an associated decrease in equivalent viscous damping had occurred. The increase was larger—or occurred in a shorter time span—than results from other studies on the natural or accelerated aging of Neoprene isolators. The changes in properties are believed to be amplified by the annular design of the isolators considered, which increases the ratio of exposed surface area to the volume of Neoprene. Although the increase in horizontal stiffness in this study may be partially attributed to the lower vertical force applied to the bearings, the increase is primarily attributed to aging effects. In spite of the considerable changes in the horizontal stiffness and damping characteristics of the bearings, the isolation system provided adequate protection for the structure throughout a large number of earthquakes; many of which constituted beyond design-basis earthquake levels that generated extreme isolator displacements.

ACKNOWLEDGMENTS

This work was supported primarily by the Earthquake Engineering Research Centers Program of the National Science Foundation under award number EEC-9701568 through the Pacific Earthquake Engineering Research Center (PEER). Any opinions, findings, and conclusions or recommendations expressed in this material are those of the author(s) and do not necessarily reflect those of the National Science Foundation.

The authors thank T. Becker and B. Olson for the design and assembly of the model, and S. Günay, S. Takhirov, and A. Schellenberg for assistance in the experimental program. The support of the Natural Sciences and Engineering Research Council of Canada (NSERC) and a Vanier Canada Graduate Scholarship is gratefully acknowledged by N.C. Van Engelen.

CONTENTS

LIST OF FIGURES

LIST OF TABLES

1 Introduction

1.1 OVERVIEW

When the original Neoprene (Polychloroprene) test series was planned, research in base isolation was at a very early stage. There were no base-isolated buildings in the United States, and the concept was met with extreme skepticism by the structural engineering profession. Shake table tests were conducted at the Earthquake Engineering Research Center (EERC) using structural models of increasing size and complexity, with fairly realistic bearings that demonstrated the feasibility of the concept. The elastomer in the bearings utilized in these tests was entirely natural rubber. Up until that time, elastomeric bridge bearings using Neoprene were limited for use as thermal expansion bearings. New interest in using Neoprene bearings for isolation applications prompted a shake table test program that used a five-story, three-bay, one-third-scale model that had already been used to test natural rubber bearings. The Neoprene bearings for this program were designed, and the Neoprene was supplied by the Polymer Products Department, Elastomers Division E.I. du Pont de Nemours & Co. Wilmington, Delaware and fabricated by Oil States Industries Inc. Athens, Texas, a very well-known bridge bearing supplier at that time.

The test program was very successful, demonstrating that there was no reason not to use Neoprene isolators for base isolation systems. Despite these findings, Neoprene has not been used in isolators in the U.S. up to the present time. Nevertheless, it has been used in several isolation projects in Armenia for a number of multi-family apartment buildings and condominiums in Yerevan, with the compound and the fabrication being made locally [Melkumyan 2011]. Its sole other use has been to isolate a number of French nuclear facilities. It is a surprising fact that the only nuclear power plants that use seismic isolation are built on Neoprene isolation bearings. These facilities include the Cruas-Messye nuclear power plant located in the south of France on the Rhone River, the La Hague Spent Fuel Storage Pools building built by Areva, and the Jules Horowitz Reactor, an experimental and medical research reactor at the CEA research site at Cadarache, France. Presently under construction at the Cadarache site is a new experimental fusion reactor, a Tokomak, called ITER which is isolated using Neoprene bearings.

The aging of this compound has been studied extensively, using accelerating aging tests following the Arrhenius approach [ASTM 2010]. Since the functionality and performance of a seismic isolation system is primarily related to low horizontal stiffness, the main emphasis on the changes with time is the shear modulus. It is accepted that the favorable properties of elastomeric isolators degrades with time as the elastomer hardens and becomes brittle due to reactions with

the environment, notably oxidation. Consequently, concern over the sensitivity of an elastomeric isolation system to aging is amplified due to uncertainty in the aged performance of the isolation system and the inherent design life of structures, which can be many decades.

This report investigates the aged horizontal behavior of Neoprene steel reinforced elastomeric isolators (SREIs) originally investigated over 30 years ago [Kelly and Hodder 1981]. The SREIs were aged unloaded at room temperature for approximately 31 years, as shown in Figure 1.1.; the findings of the original study are reviewed herein. A similar experimental program was conducted to ascertain the sensitivity of the Neoprene isolators to aging effects and to study the dynamic behavior at inputs that constitute beyond design-basis earthquake levels.

Figure 1.1 Isolator storage conditions.

1.2 AGING OF NEOPRENE ISOLATOR BEARINGS

The exterior surface of the isolator is most affected by aging due to the higher level of exposure to the environment and subsequent oxidation. Thus, the region with the largest variation in material properties occurs at the exterior surface of the isolator. The variation in material properties gradually decreases, moving inwards from the exterior surface to the interior region of the elastomer and past the critical depth, which is not affected by oxidation. The permeability of the exterior oxidized region in natural rubber is substantially reduced, which acts as a mechanism to prevent further oxidation of the interior region of the isolator [Itoh and Gu 2009]. Intuitively, smaller isolators are more sensitive to aging due to the larger ratio of exposed surface area to the volume of the elastomer. This was demonstrated experimentally utilizing accelerated aging by Yura et al. [2001] for Shore A 50 and 70 durometer natural rubber and Neoprene specimens. The study considered three different sizes of square specimens with lengths between 1 in. (25.4 mm) and 3 in. (76.2 mm). The accelerated aging caused an increase in stiffness between about 20% to 60% depending on the hardness and the size of the specimen. Translating the accelerated aging to natural aging at ambient temperatures, the study concluded that it would take hundreds of years for the observed increase to occur through natural aging at ambient temperatures.

Coladant [1993] investigated the aging of neoprene isolators used in the Cruas-Messye nuclear power plant. After approximately 11 years of natural aging, the shear modulus increased by about 25%. From the limited data available it was predicted that the shear modulus would

increase by a maximum of 37%. Accelerated aging tests on samples of the compound were also carried out. The samples were placed in a heated chamber at 70°C for ten weeks, with samples regularly tested for the dynamic modulus and damping. These tests showed that the shear modulus would increase at most by 25%; the damping appeared to decrease by about 10%, but the trend was less clear.

Russo et al. [2013] considered the accelerated aging of unbonded fiber-reinforced Neoprene elastomeric isolators. It was noted that the code used for the accelerated aging did not indicate the representative age of the treated specimens. A maximum increase in the horizontal stiffness of 17% at a shear strain of 1.0 and decrease in equivalent viscous damping of 20% was observed in the study.

2 Review of 1981 Investigation

2.1 BACKGROUND

The original experimental program presented in Kelly and Hodder [1981] was conducted to demonstrate the feasibility of seismic isolation for structures and the suitability of elastomeric isolators. This was demonstrated through a series of shake table experiments on a scaled model, with the addition of static testing to investigate the horizontal and vertical properties of the annular isolators. The one-third scale model used in the shake table experiments was a five-story, three-by-one bay steel frame shown in Figure 2.1. Each of the four corners of the steel frame was supported on a bearing and base floor girders connected the unsupported columns to the bearings. The total weight of the model was 80 kip (356 kN), which includes the self-weight of the frame and additional dead load.

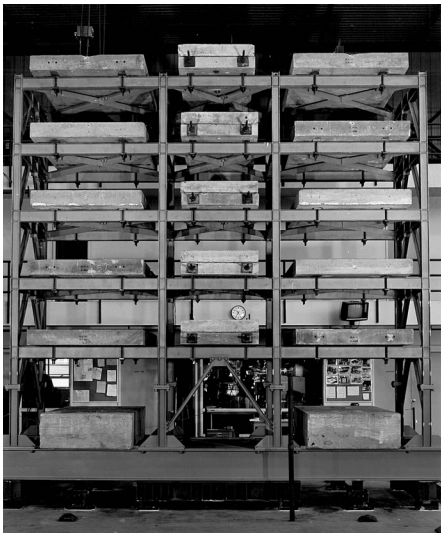

Figure 2.1 One-third scale structure from Kelly and Hodder [1981].

2.2 SPECIMENS

The central hole of the annular isolators was provided to facilitate the use of elastomeric and lead cores in the original study. Only the properties of the unfilled configuration are considered for comparative purposes in this investigation. The isolators were designed by the Polymer Products

Department, Elastomers Division of E.I. du Pont de Nemours & Co. (Inc.), in Wilmington, Delaware, and manufactured and donated by Oil States Industries Inc., Athens, Texas.

Two Neoprene elastomers were used, one with a Shore A 40 durometer hardness and the other with a 50 durometer hardness, henceforth referred to simply as 40A and 50A isolators. The multi-layer isolators were manufactured with 44 layers of elastomer and 43 layers of steel reinforcement. Each layer of Neoprene was approximately 0.057 in. (1.4 mm) thick and the total thickness of the elastomeric layers was 2.5 in. (63.5 mm). Each layer of steel reinforcement was approximately 0.060 in. (1.5 mm) thick. Two square steel end plates, each with a thickness of 0.25 in. (6.4 mm) and a width and length of 7 in. (177.8 mm), were used to mechanically fasten the isolator to the substructure and superstructure. The total height of the isolator was 5.5 in. (139.7 mm). The outside diameter was 5.5 in. (139.7 mm) and the inside diameter was 2.0 in. (50.8 mm). The annular isolators had a total plan area of 20.6 in^2 (13,290 mm^2). Figure 2.2 shows a cross section of the specimen, emphasizing the high shape factor of 15.4 represented by the thin layers of elastomer in comparison to the loaded area and the large aspect ratio of the bearing. These bearings were not well proportioned even when originally produced, but the shape was necessary to provide the low stiffness required for the period of the isolated structure.

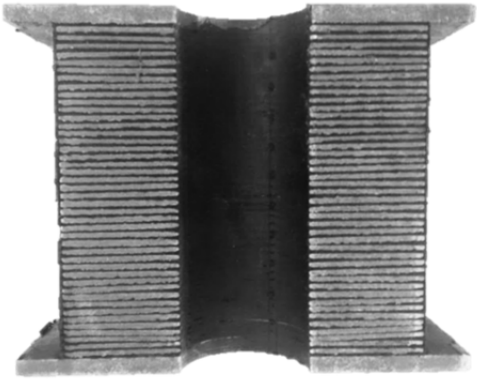

Figure 2.2 Profile cross section of an annular SREI specimen.

2.3 STATIC TESTING

The isolators were initially statically tested in tandem and with unfilled cores. A vertical compressive force of 20 kip (89 kN) was applied, corresponding to the average weight on each isolator in the model. The horizontal stiffness of a single 50A isolator was approximately 1.0 kip/in. (0.175 kN/mm) at zero horizontal displacement. It was observed that the horizontal stiffness steadily decreased with increasing displacement, decreasing to 0.4 kip/in. (0.070 kN/mm) at a horizontal displacement of 2.0 in. (50.8 mm), corresponding to a shear strain of 0.80. The static vertical stiffness under a vertical compressive force of 20.0 kip (89.0 kN) was 420 kip/in. (74 kN/mm) and 600 kip/in. (105 kN/mm) for the 40A and 50A isolator, respectively. A critical load of 33.4 kip (149 kN) was experimentally determined at zero horizontal displacement for the 40A isolator; this was 38% lower than the critical load of 53.8 kip (239 kN) carried by the 50A isolator.

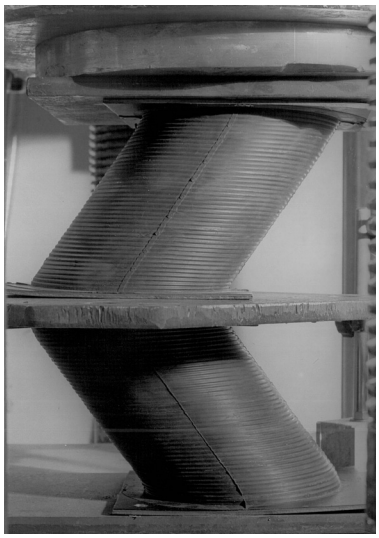

Figure 2.3 Static horizontal test with the bearings in tandem [Kelly and Hodder 1981].

2.4 DYNAMIC TESTING

The dynamic shake table test program considered four historic California earthquake records that had occurred prior to 1981. The earthquake records were complimented with numerous pullback tests where the model was initially displaced and suddenly released in free vibration. From the pullback tests, a fixed-base fundamental frequency of 3.9 Hz was determined. The fundamental frequency of the model, base isolated with 40A and 50A isolators, was 0.50 Hz and 0.75 Hz, respectively. Based on the fundamental frequency, the horizontal stiffness of the 40A isolators was determined to be 0.50 kip/in. (0.088 kN/mm) and 1.15 kip/in. (0.201 kN/mm) for the 50A isolators. It was noted that the dynamically obtained horizontal stiffness for the 50A isolator was 15% higher than determined statically at zero horizontal displacement.

The horizontal force-displacement hysteresis loops at the peak isolator displacement in the El Centro record from the 1940 Imperial Valley earthquake with a peak ground acceleration (PGA) of 0.54*g* are presented in Figure 2.4. The hysteresis loops are reproduced from Kelly and Hodder [1981]. The equivalent viscous damping of the system was 11% and 10% for the 40A and 50A isolators, respectively. In all cases the isolation mode dominated the response of the model, and the structure responded in near rigid motion on top of the isolation system. The fixed-base structure amplified the table acceleration of 0.54*g* to a peak absolute acceleration of 1.9*g* at the fifth floor of the structure. Both the 40A and 50A isolation systems resulted in a substantial decrease in peak absolute acceleration. The 40A isolator, which had a lower horizontal stiffness, provided a larger decrease in peak absolute acceleration to 11% of the table acceleration. The 50A isolator had a peak absolute acceleration of roughly 0.1*g* or 19% of the table acceleration. Similar large decreases in peak absolute acceleration of the structure were obtained for the other earthquake records considered.

The 40A bearings had a lower peak isolator displacement than the 50A bearings for the same table input. This was unexpected as the period was significantly larger and displacements

are generally expected to increase with period. However, in these tests it is probable that the input signal was filtered to keep the table displacement within the table capacity, consequently reducing the isolator displacement.

The maximum displacement capacity of the 50A isolators was evaluated by increasing the peak table acceleration to 0.68*g* and 0.835*g*. The peak isolator displacement was 2.5 in. (63.5 mm) at a peak table acceleration of 0.54*g*. By increasing the peak table acceleration to 0.68*g*, the peak isolator displacement increased to 3.5 in. (88.9 mm), but the peak absolute acceleration of the frame was relatively unaffected. At the maximum considered table acceleration of 0.835*g*, the peak displacement was 4.2 in. (106.7 mm); only a minor increase in the peak absolute acceleration of the frame was observed. The small change in peak absolute acceleration of the frame was attributed to a favorable softening and increase in damping in the isolators. This softening and increase in damping, as shown in Figure 2.5, was larger where an increase in vertical compressive force occurred due to overturning moments. The horizontal stiffness of SREIs decreases with increasing horizontal displacement [Buckle et. al 2002]. Although significant critical load carrying capacity exists as the horizontal displacement approaches the diameter of the bearing, the combination of large displacements and increased vertical compressive force amplifies the softening [Nagarajaiah and Ferrell 1999]. Consequently, under these conditions, the isolator approaches the stability limit as observed in the Southwest isolator.

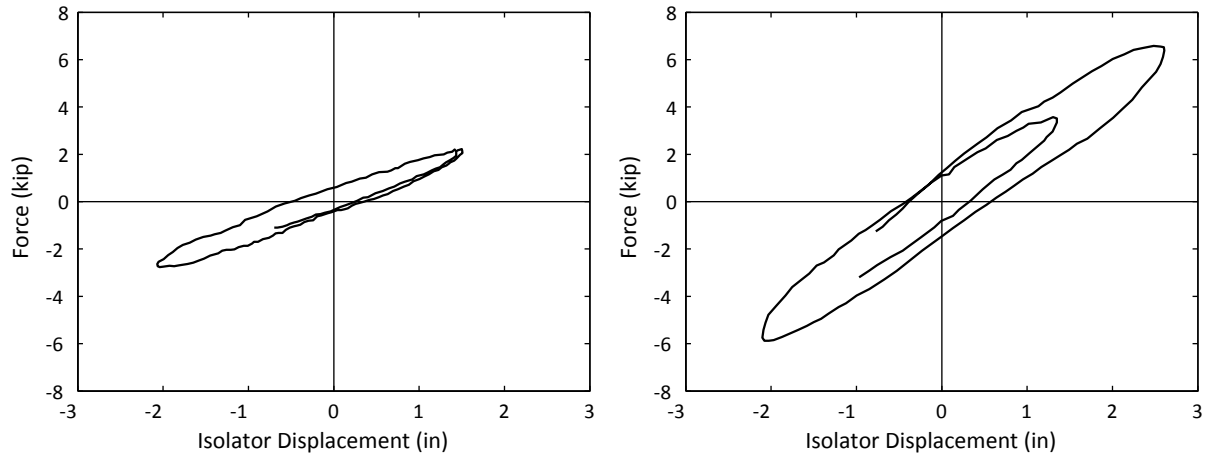

Figure 2.4 **Peak isolator displacement hysteresis loops from the Imperial Valley earthquake (PGA = 0.54*g*) of the (a) 40A and (b) 50A isolators [Kelly and Hodder 1981].**

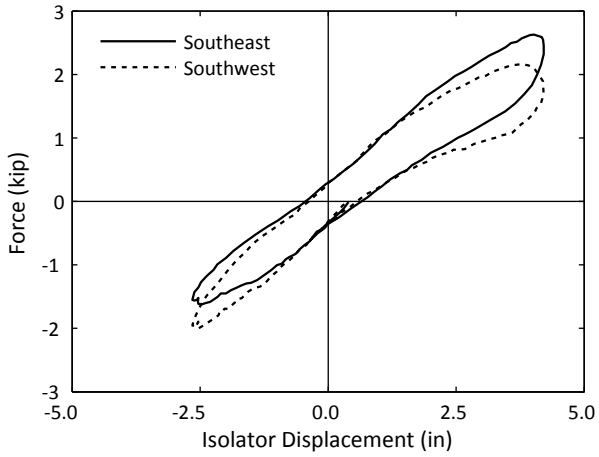

Figure 2.5 **Comparison of the hysteresis loops from the Imperial Valley earthquake (PGA = 0.835*g*) of the Southeast and Southwest isolators [Kelly and Hodder 1981].**

3 2012 Investigation

3.1 EXPERIMENTAL SET-UP

The experimental tests were conducted on a single-degree-of-freedom stiff platform assembly on a linear bearing system known as the Real-Time Hybrid Simulation Platform. The Real-Time Hybrid Simulation Platform was powered by a high-performance 150 kip (667 kN) actuator with a ±20 in. (±508 mm) stroke limit. The one-third scale superstructure was a two story, two-by-one bay steel frame assembled from the NEES REPEAT system, with a total weight of 87 kip (387 kN) including the additional blocks added to simulate dead load. Six isolators were considered simultaneously, with one located under each column of the frame. The isolators were stored for 30 years; some were still in the original wrapping. Over this time period the identity of the 40A and 50A isolators was lost and not identified until load cells under each individual isolator revealed the type. The isolator layout, identifying the location of the 40A and 50A isolators in the model, is provided in Figure 3.1.

Each specimen was mechanically fixed on top of a five-component load cell, as shown in Figure 3.2a. The experiments were conducted with a rigid and flexible superstructure configuration. The rigid configuration was implemented by utilizing the safety system to stiffen the superstructure and prevent deformations. In the flexible configuration, the safety system was used only to prevent the collapse of the superstructure. The experimental model is shown in Figure 3.2b.

The average vertical compressive force of 14.5 kip (64.5 kN) per isolator was 73% of the average vertical compressive force applied to each isolator in the original study. It was found that the total weight of the model was not evenly distributed to the isolators, with significant variation along the South side of the model. The South 40A isolator carried about 29% of the total weight, whereas the Southeast and Southwest isolators carried approximately 12% and 9% of the total weight, respectively. The distribution along the North side of the model was more uniform, with each isolator carrying approximately 17% of the total weight.

Pullback tests of the model in the flexible configuration and in a fixed-base condition were conducted by applying an 8.0 kip, (36 kN) force to the third level of the frame and instantaneously releasing the load, which allowed the structure to enter free vibration. The fundamental frequency of the frame was determined to be 2.0 Hz with approximately 1.4% damping; a displacement time history of Level 3 from a pullback test is shown in Figure 3.3.

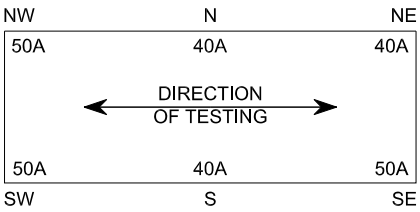

Figure 3.1 **Plan view of the isolator layout.**

(a) **(b)**

Figure 3.2 **Experimental apparatus: (a) a SREI specimen mechanically fixed to the supports, and (b) the NEES REPEAT system (blue) and additional dead load (white).**

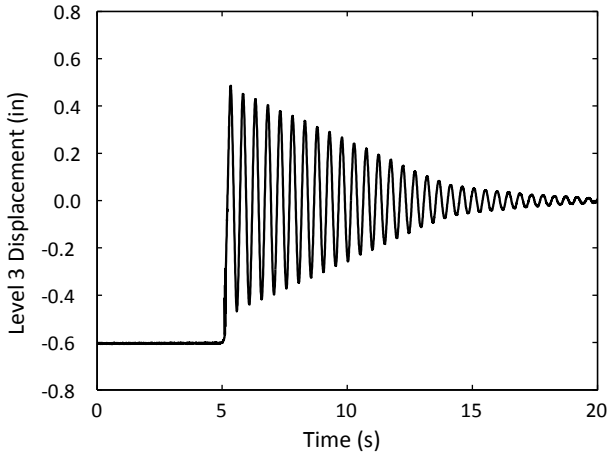

Figure 3.3 **Fixed-base pullback test Level 3 displacement time history.**

3.2 TEST PROTOCOL

3.2.1 Input Earthquake Records

Four historical earthquake records and one synthetic record were selected for this study. The four historical records are from the Imperial Valley (1940), Superstition Hills (1987), Loma Prieta (1989), and Northridge (1994) earthquakes; see Table 3.1. To maintain dynamic similitude in the experimental program, the time component of each historical record was compressed by a factor of $\sqrt{3}$ based on the one-third scale model. Throughout the test program, the intensity of the earthquake was changed by scaling the peak ground acceleration (PGA) ,as discussed in the subsequent section. Figure 3.4 shows the acceleration time history of each earthquake scaled to a PGA of 0.5*g*; Figure 3.5 provides the corresponding spectral acceleration, S_a, at an equivalent viscous damping, ζ, of 2%, 5%, and 10%. Note that a comparison of the spectral accelerations shows that the synthetic record, TestQke4IEEE, had a significantly larger spectral acceleration at longer periods than the historical records considered.

The TestQke4IEEE record was generated using response spectrum matching time domain procedures, as described in Takhirov et al. [2004]. The synthetic record is derived from the Landers (1992) earthquake Joshua Tree record and is intended to match the required response spectrum for the shake-table testing of non-structural equipment, such as AC156 [ICC-ES 2010] and IEEE693 [IEEE 2006]. This study considered the *x*-component of the earthquake. The TestQke4IEEE record was only conducted in the flexible configuration and was not scaled to simulate base-isolated equipment to full-scale ground motions.

Table 3.1 Selected historical earthquake records.

Earthquake	Date	Station	Direction
Imperial Valley	5/19/1940	177 El Centro Array #9	180
Superstition Hills	11/24/1987	11369 Westmorland Fire Station	180
Loma Prieta	10/18/1989	57382 Gilroy Array #4	0
Northridge	1/17/1994	655 Jensen Filtration Plant	22

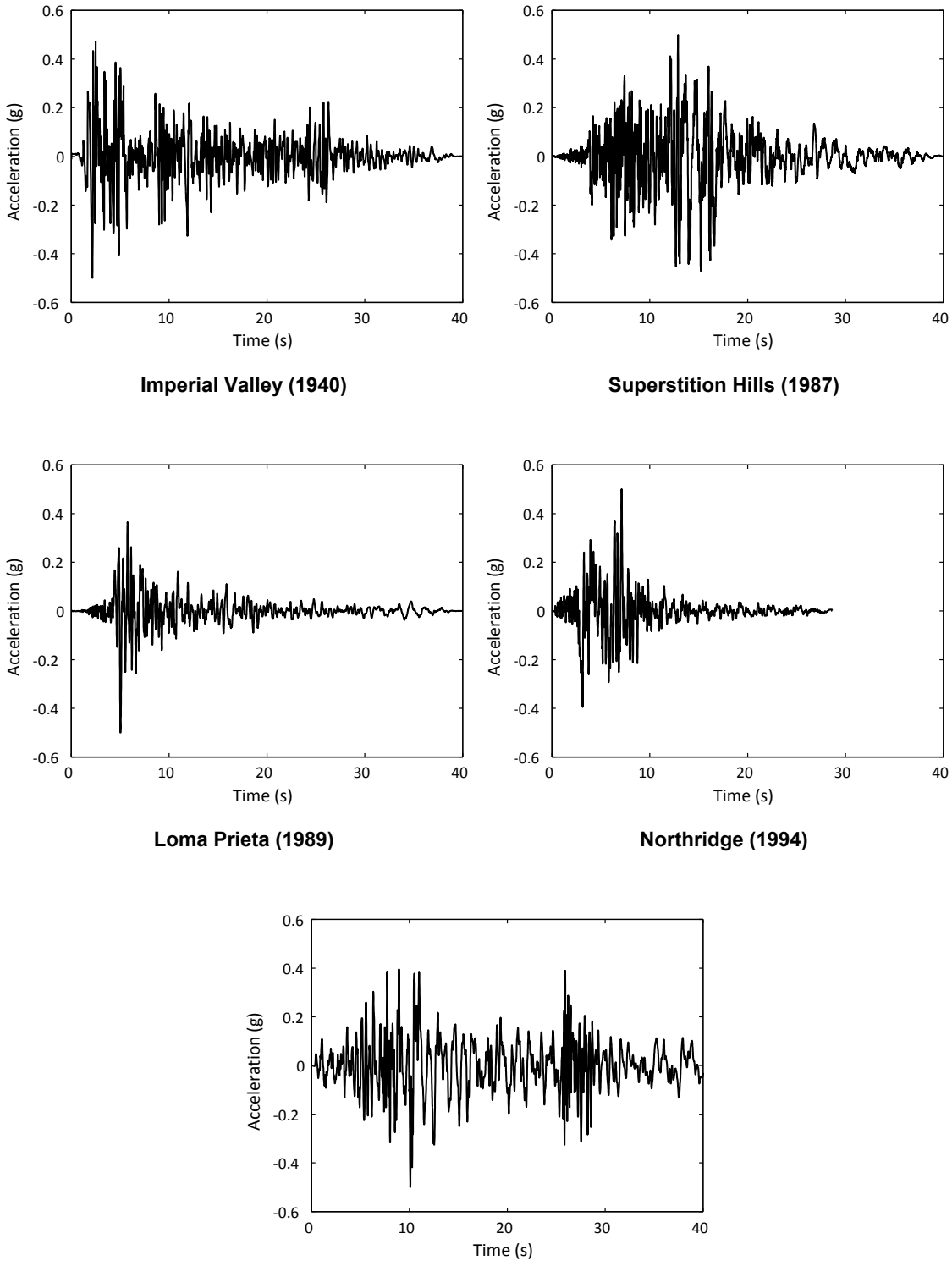

Figure 3.4 Full-scale acceleration time histories (PGA = 0.5*g*).

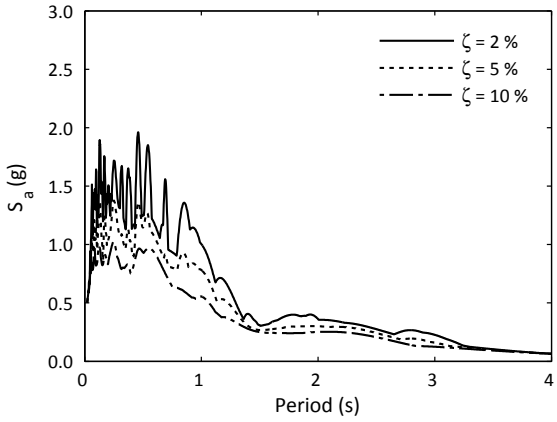

Imperial Valley (1940)

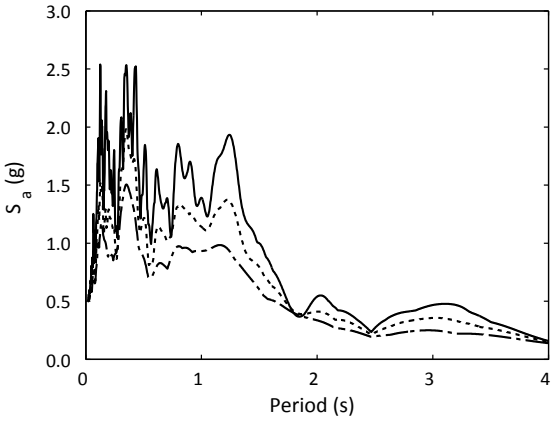

Superstition Hills (1987)

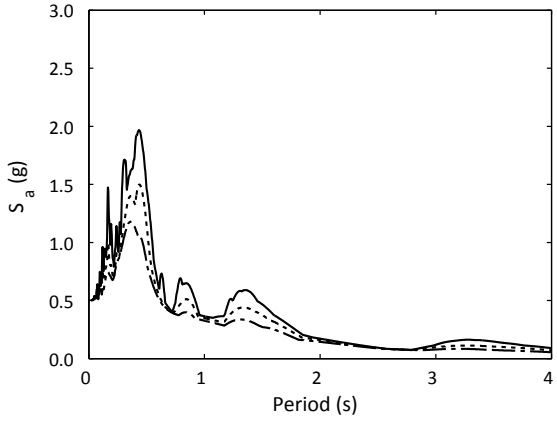

Loma Prieta (1989)

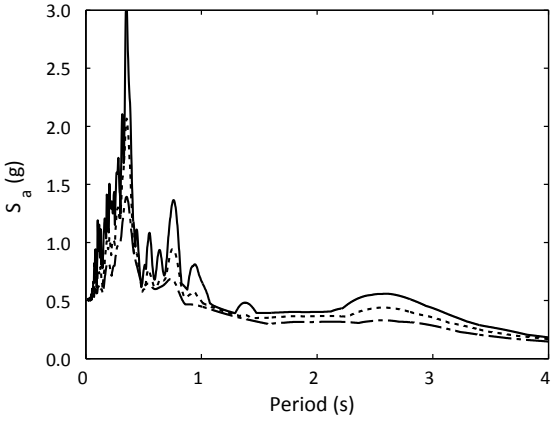

Northridge (1994)

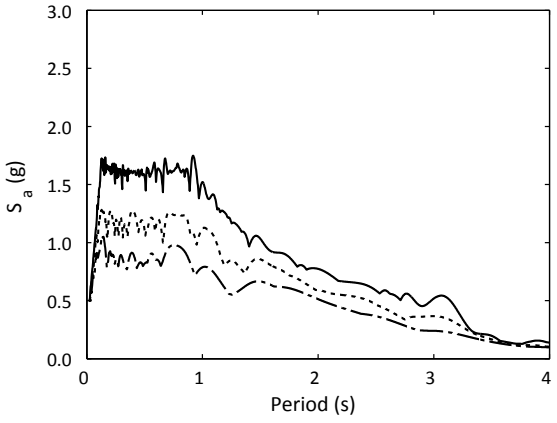

TestQkelEEE

Figure 3.5 Full-scale spectral accelerations (PGA = 0.5*g*).

3.2.2 Test Program

The experimental test program consisted of pullback tests, earthquake records, and acceleration sinusoidal sweeps. Only the pullback tests and earthquake records are considered in this study. Unlike the pullback tests conducted to determine the fixed-base properties of the model structure, the base-isolated pullback tests were conducted by instantaneously releasing the model from an initial displacement at the isolation layer. Initial displacements between 1.0 in. (25.4 mm) and 2.0 in. (50.8 mm) were considered; see Table 3.2.

The experimental program of the historical earthquake records is provided in Table 3.3. A total of 45 historical earthquake runs were conducted. Provided in the table is the measured peak ground (table) displacement (PGD) and peak ground (table) acceleration obtained during each test, corresponding to the one-third-scale model. The order of the runs represents the sequence that the tests were conducted for each earthquake; however, all rigid (R) configuration runs were completed prior to the flexible (F) configuration runs. A maximum PGA of 0.67*g*, 0.50*g*, 1.16*g*, and 0.29*g* were measured for the Imperial Valley, Superstition Hills, Loma Prieta, and Northridge earthquakes, respectively. The TestQke4IEEE experimental results are summarized in Table 3.4. Note that these runs were conducted at full scale; therefore, the PGD is representative of full-scale displacements. Details on the experimental test sequence are provided in Appendix A.

Table 3.2 Pullback experimental program.

Run	Configuration	Initial Displacement	
		(in.)	(mm)
1	R	1.0	25.4
2		1.2	30.5
3		1.5	38.1
4		1.5	38.1
5	F	1.5	38.1
6		1.5	38.1
7		2.0	50.8

Table 3.3 Historical earthquake experimental program.

Earthquake	Run	Configuration	PGD		PGA	Earthquake	Run	Configuration	PGD		PGA
			(in.)	(mm)	(*g*)				(in.)	(mm)	(*g*)
Imperial Valley	1	R	0.26	7	0.15	Loma Prieta	1	R	0.25	6	0.12
	2		0.51	13	0.21		2		0.49	13	0.20
	3		0.75	19	0.37		3		0.83	21	0.34
	4		1.00	26	0.45		4		1.28	33	0.48
	5		1.25	32	0.54		5	F	0.49	12	0.19
	6		1.25	32	0.54		6		0.83	21	0.32
	7		1.50	38	0.67		7		1.28	32	0.46
	8		1.50	38	0.65		8		1.66	42	0.63
	9	F	0.26	7	0.16		9		1.92	49	0.77
	10		0.50	13	0.22		10		2.11	53	0.82
	11		0.75	19	0.34		11		2.32	59	0.99
	12		1.00	25	0.45		12		2.66	68	1.10
	13		1.25	32	0.52		13		2.93	74	1.16
	14		1.50	38	0.61		14		1.67	42	0.63
							15		2.66	68	1.07
Superstition Hills	1	R	0.26	7	0.09	Northridge	1	R	0.25	6	0.08
	2		0.51	13	0.13		2		0.50	13	0.17
	3		0.86	22	0.18		3		0.65	17	0.17
	4		1.45	37	0.31		4		1.11	28	0.24
	5		2.26	57	0.50		5		1.30	33	0.29
	6	F	0.86	22	0.19		6	F	0.66	17	0.18
	7		1.45	37	0.30		7		1.11	28	0.24
	8		2.26	57	0.50		8		1.23	31	0.23

Table 3.4 TestQke4IEEE experimental program.

Run	Configuration	PGD		PGA
		(in.)	(mm)	(*g*)
1	F	0.33	8	0.07
2		0.65	17	0.12
3		1.30	33	0.17
4		1.47	37	0.20
5		1.30	33	0.19

4 Experimental Results

4.1 AGING EFFECTS

4.1.1 Comparison between Isolators

4.1.1.1 40A Isolators

Figure 4.1a shows the effective horizontal stiffness, k_{eff}, of the rigid and flexible configurations as a function of the peak isolator displacement of the Imperial Valley runs. The effective horizontal stiffness presented was determined from the cycle over which the peak isolator displacement occurs. The minimum peak isolator displacement was 0.39 in. (9.9 mm), and the maximum peak isolator displacement was 3.01 in. (76.5 mm) over Imperial Valley Run 1 and Run 7, respectively. A softening trend occurred with increasing peak isolator displacement. A maximum effective horizontal stiffness of 0.91 kip/in. (0.159 kN/mm) occurred at the minimum peak isolator displacement of 0.39 in. (9.9 mm) in the Northeast isolator. The effective horizontal stiffness decreased by 35% to a minimum stiffness of 0.59 kip/in. (0.103 kN/mm) at the maximum peak displacement of 3.01 in. (76.5 mm). Similar to the Northeast isolator, the effective horizontal stiffness of the South isolator decreased over the range of peak isolator displacement by 36%, from 0.66 kip/in. (0.116 kN/mm) to 0.40 kip/in. (0.70 kN/mm). The effective horizontal stiffness varied significantly between the three 40A isolators. Table 4.1 shows the mean, μ, and coefficient of variation, c_v, at all levels of peak isolator displacement in ascending order. The c_v is relatively consistent, ranging between 0.16 and 0.21, but it is representative of the large variation observed in the effective horizontal stiffness.

The equivalent viscous damping was found to increase with increasing peak isolator displacement as compared in Figure 4.1b. The South isolator, which had the lowest horizontal stiffness, had the highest damping, ranging from 9.0% to 11.6% at a peak isolator displacement of 0.39 in. (9.9 mm) and 3.01 in. (76.5 mm), respectively. The damping in the South isolator was considerably higher than the North or Northeast isolator, which varied between 4.6% at a peak isolator displacement of 0.39 in. (9.9 mm) in the Northeast isolator, and 7.4% at 3.01 in. (76.5 mm) in the North isolator. Figure 4.2 highlights the difference in effective horizontal stiffness and damping between the Northeast and South isolator. The higher damping in the South isolator is partially attributed to the lower effective horizontal stiffness. However, from the hysteresis loops it can be determined that the area enclosed within the loops is 26% greater for this isolator. This suggests that the energy dissipation characteristics of the South isolator were greater than the Northeast or North isolator.

Table 4.1 Summary of k_{eff} from the Imperial Valley runs.

Run	PGA (*g*)	Peak isolator displacement		40D			50D		
		(in.)	(mm)	μ (kip/in.)	μ (kN/mm)	c_v	μ (kip/in.)	μ (kN/mm)	c_v
1	0.15	0.39	9.9	0.81	0.141	0.16	1.69	0.297	0.03
9	0.16	0.42	10.6	0.71	0.125	0.18	1.54	0.271	0.06
2	0.21	0.82	20.9	0.69	0.121	0.20	1.46	0.256	0.03
10	0.22	0.91	23.0	0.63	0.110	0.20	1.34	0.234	0.06
3	0.37	1.32	33.5	0.64	0.112	0.18	1.31	0.230	0.03
11	0.34	1.43	36.3	0.57	0.101	0.21	1.22	0.213	0.06
4	0.45	1.86	47.2	0.60	0.104	0.17	1.20	0.211	0.03
12	0.45	1.96	49.9	0.54	0.095	0.20	1.12	0.197	0.06
5	0.54	2.43	61.8	0.55	0.096	0.17	1.10	0.192	0.02
6	0.54	2.47	62.6	0.54	0.094	0.18	1.08	0.189	0.03
13	0.52	2.48	63.1	0.51	0.089	0.20	1.05	0.184	0.06
14	0.61	2.99	75.9	0.48	0.084	0.21	0.99	0.173	0.05
8	0.65	3.00	76.1	0.49	0.086	0.20	0.99	0.173	0.02
7	0.67	3.01	76.6	0.50	0.088	0.19	1.01	0.177	0.02

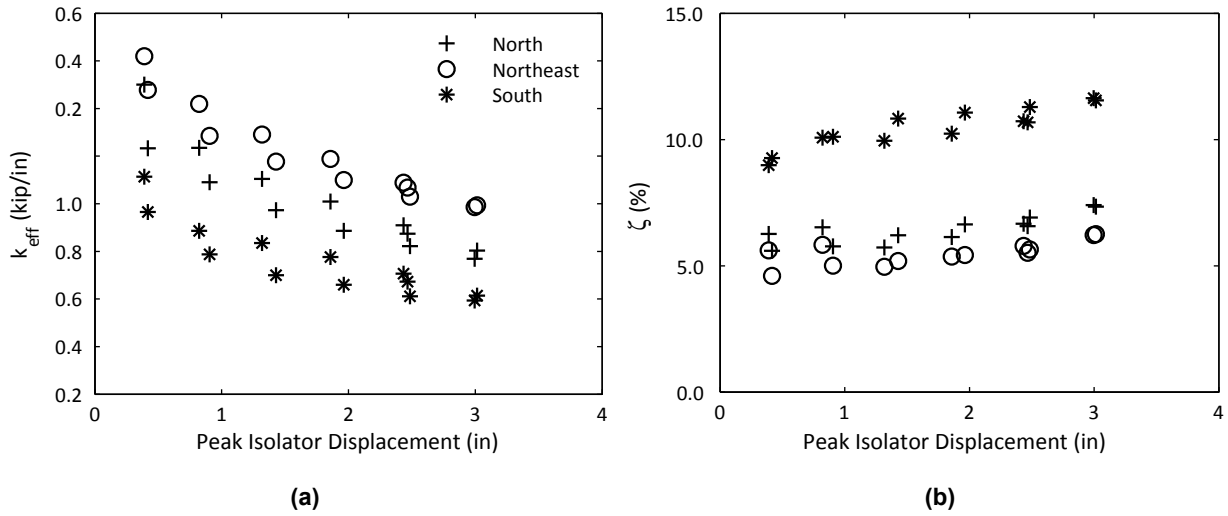

Figure 4.1 **Comparison of the (a) effective horizontal stiffness and (b) the equivalent viscous damping as a function of peak isolator displacement obtained from the Imperial Valley runs for the 40A isolators.**

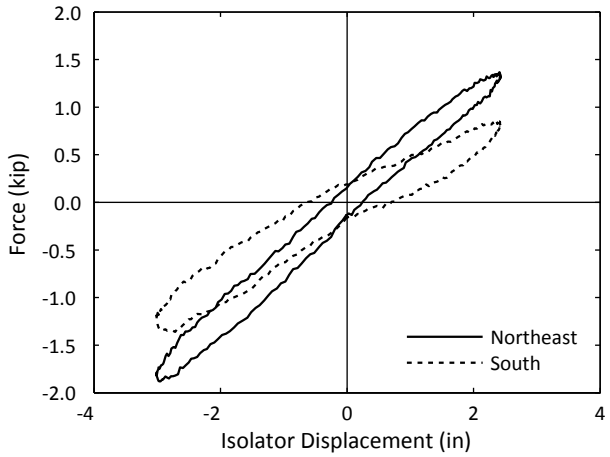

Figure 4.2 **Comparison of the peak isolator displacement hysteresis loops from Imperial Valley Run 7 (PGA = 0.67*g*) of the Northeast and South 40A isolators.**

4.1.1.2 50A Isolators

Figure 4.3a compares the effective horizontal stiffness as a function of the peak isolator displacement obtained from the Imperial Valley runs. Similar to the 40A isolators, a softening trend occurred with increasing peak isolator displacement. At a peak isolator displacement of 0.39 in. (9.9 mm), the effective horizontal stiffness ranged between 1.66 kip/in. (0.291 kN/mm) and 1.74 kip/in. (0.305 kN/mm) for the Northwest and Southwest isolator, respectively. The effective horizontal stiffness decreased by 41% and 43% at 3.01 in. (76.5 mm) peak isolator displacement for the Northwest and Southwest isolator, respectively. A minimum effective horizontal stiffness of 0.97 kip/in. (0.170 kN/mm) was observed in the Northwest isolator. The variation in the effective horizontal stiffness was considerably lower in the 50A isolators than the

40A isolators. The c_v ranged between 0.02 and 0.06 compared to the range of 0.16 to 0.21 of the 40A isolators (see Table 4.1).

As shown in Figure 4.3b, the consistency of the equivalent viscous damping is comparable to the consistency of the effective horizontal stiffness. In constrast to the 40A isolators, in which the damping generally increased with increasing peak displacement, the damping in the 50A isolators decreased slightly before increasing. A minimum damping of 5.2% in the Northwest isolator was observed at 1.32 in. (33.5 mm) peak isolator displacement in Imperial Valley Run 3. A maximum damping of 7.0% occurred at a peak isolator displacement of 3.01 in. (76.5 mm) in the Southwest isolator. Figure 4.4 compares the hysteresis of the Southwest and Northwest isolators. The hysteresis loops are comparable both in peak force and area contained within the loops, reinforcing the high consistency observed in the effective horizontal stiffness and equivalent viscous damping.

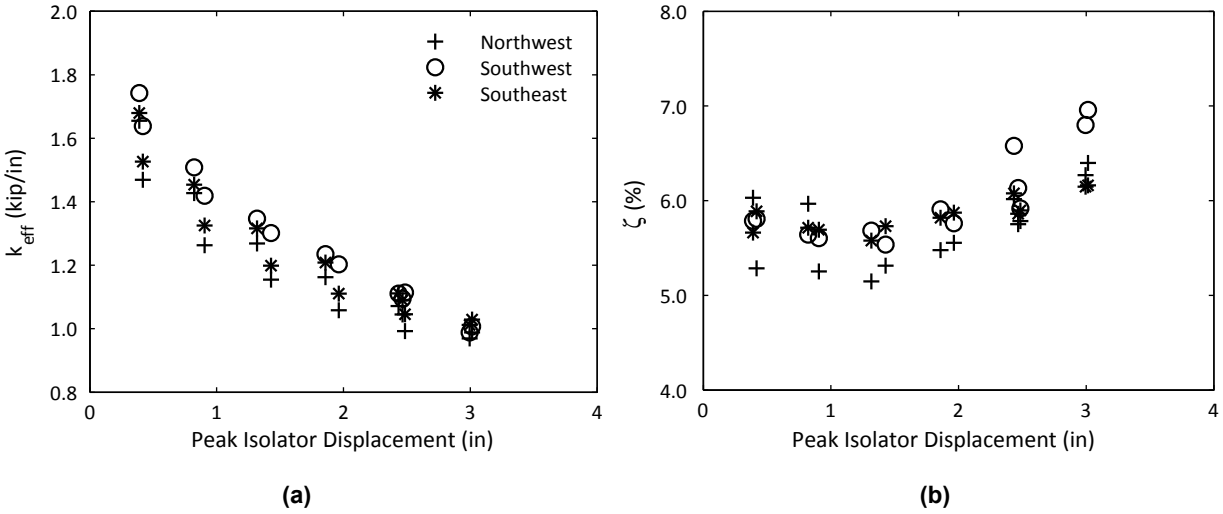

Figure 4.3 **Comparison of the (a) effective horizontal stiffness and (b) the equivalent viscous damping as a function of peak isolator displacement obtained from the Imperial Valley runs for the 50A isolators.**

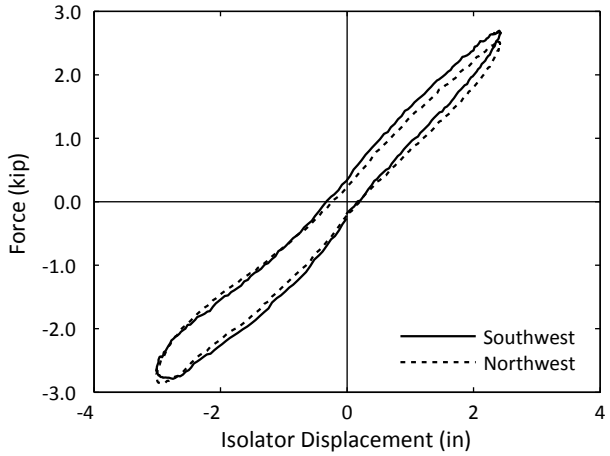

Figure 4.4 **Comparison of the peak isolator displacement hysteresis loops from Imperial Valley Run 7 (PGA = 0.67 g) of the Northwest and Southwest 50A isolators.**

4.1.2 Comparison between Isolators: Then and Now

4.1.2.1 40A Isolators

The average effective horizontal stiffness of a 40A isolator obtained during the Imperial Valley runs was 0.35 kip/in. (0.061 kN/mm) with 11.3% damping. Figure 4.5 compares the average hysteresis of a 40A isolator from Kelly and Hodder [1981] to the hysteresis of the South 40A isolator presented in this study. The hysteresis was selected from Imperial Valley Run 4 to approximately match the peak displacements of the cycle presented in the original study. Results indicate that significant stiffening occurred over the time period despite the comparatively low effective horizontal stiffness of the South isolator. The effective horizontal stiffness of 0.49 kip/in. (0.086 kN/mm) was 40% greater than observed in the original study. The mean effective horizontal stiffness of the selected cycle was 0.60 kip/in. (0.105 kN/mm); an increase of 72%.

The equivalent viscous damping was approximately equal at 10.2% and 11.3% for the current and original study, respectively. Note that the South 40A isolator was found to have significantly higher damping than either the North or Northeast 40A isolator. Over the cycle presented in Figure 4.5, the damping was 6.2% and 5.4% in the North and Northeast 40A isolator, respectively. Comparing these values to the damping of 11.3% from the original study, the damping in the North and Northeast isolators decreased by 45% and 52%, respectively.

The isolator displacement and force time history from the Imperial Valley earthquake with 40A isolators and a PGA of 0.534*g* from Kelly and Hodder [1981] is reproduced in Figure 4.6. The time histories are compared to the results of Imperial Valley Run 12 (PGA = 0.45*g*). The peak isolator displacement of 1.96 in. (49.8 mm) from Imperial Valley Run 12 was selected to approximately match the peak isolator displacement of 2.08 in. (52.8 mm) from Kelly and Hodder [1981]. It can be seen that the peak response of both time histories occur between 4 sec and 8 sec, although the peak displacements occur in opposing directions and at different times. The mean force time histories (Figure 4.6b) indicate that the force increased for approximately equal displacements, which is representative of the stiffening observed in the hysteresis loops.

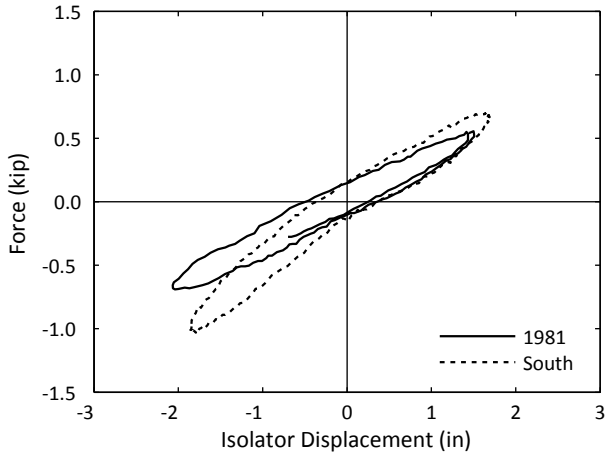

Figure 4.5 **Comparison of the average hysteresis loop of the 40A isolator presented in Kelly and Hodder [1981] and the South 40A isolator presented in the current study from Imperial Valley Run 4 (PGA = 0.45*g*).**

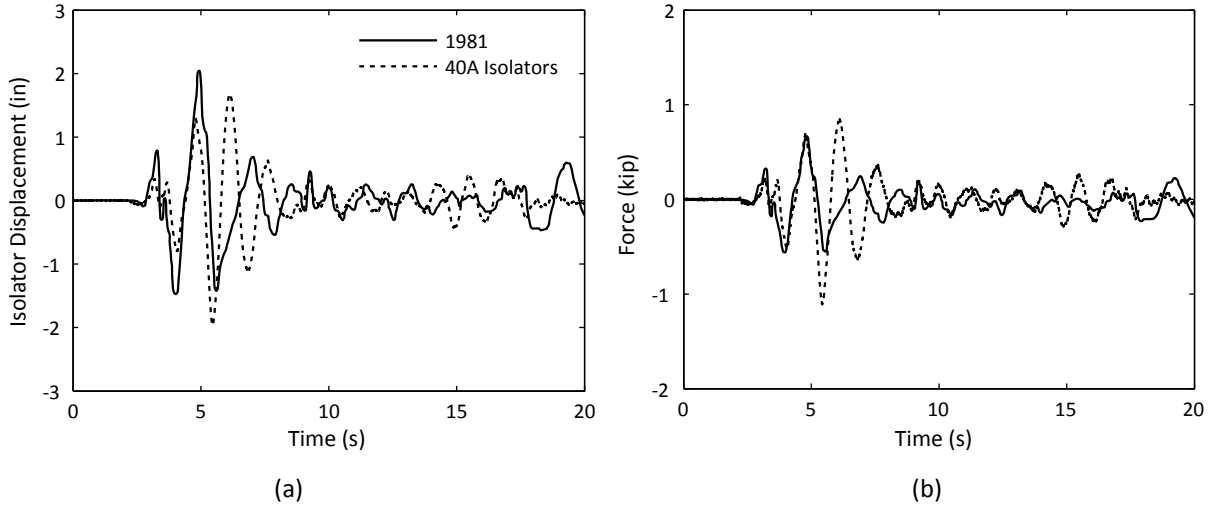

Figure 4.6 **Comparison of the Imperial Valley (PGA = 0.534*g*): (a) isolator displacement and (b) mean force time histories presented in Kelly and Hodder [1981] to Imperial Valley Run 12 (PGA = 0.45*g*).**

4.1.2.2 50A Isolators

The average effective horizontal stiffness of the 50A isolators from the Imperial Valley earthquake in Kelly and Hodder [1981] was 0.66 kip/in. (0.116 kN/mm). Figure 4.7 compares the hysteresis from the original study to the Southwest 50A isolator from Imperial Valley Run 5, highlighting the large increase in effective horizontal stiffness. The effective horizontal stiffness in the Southwest 50A isolator increased by 68% to 1.11 kip/in. (0.195 kN/mm). The mean effective horizontal stiffness of the selected cycle was 1.10 kip/in. (0.193 kN/mm), increasing by 67%. The damping decreased by a mean of 50%, from 12.3% to 6.2%, which is comparable to the decrease observed in the North and Northeast 40A isolators.

The displacement time histories of the Imperial Valley earthquake with 50A isolators and a PGA of 0.543*g* from Kelly and Hodder [1981] shows good agreement with Imperial Valley Run 5 (PGA = 0.54*g*) with respect to the peak response in the 4 sec to 8 sec range, as shown in Figure 4.8. The peak positive displacement was 2.07 in. (52.6 mm) and 2.09 in. (53.1 mm) and the peak negative displacement was 2.43 in. (61.7 mm) and 2.59 in. (65.7 mm) for the original and current study, respectively. At these respective peak displacements the mean 50A isolator force was 1.48 kip (6.6 kN), 2.36 kip (10.5 kN); and 1.66 kip (7.4 kN) and 2.58 kip (11.5 kN). These values correspond to an increase of 59% at the peak positive displacement, and 57% at the peak negative displacement. This indicates a lower but comparable increase in stiffness than was observed in the hysteresis loops comparison.

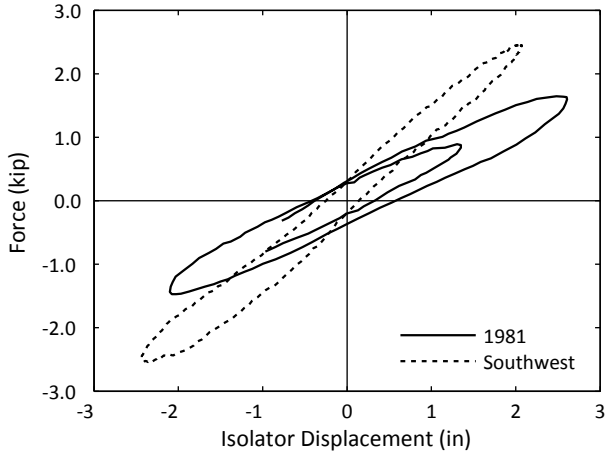

Figure 4.7 Comparison of the average hysteresis loop of the 50A isolator presented in Kelly and Hodder [1981] and the Southwest 50A isolator presented in the current study from Imperial Valley Run 5 (PGA = 0.54*g*).

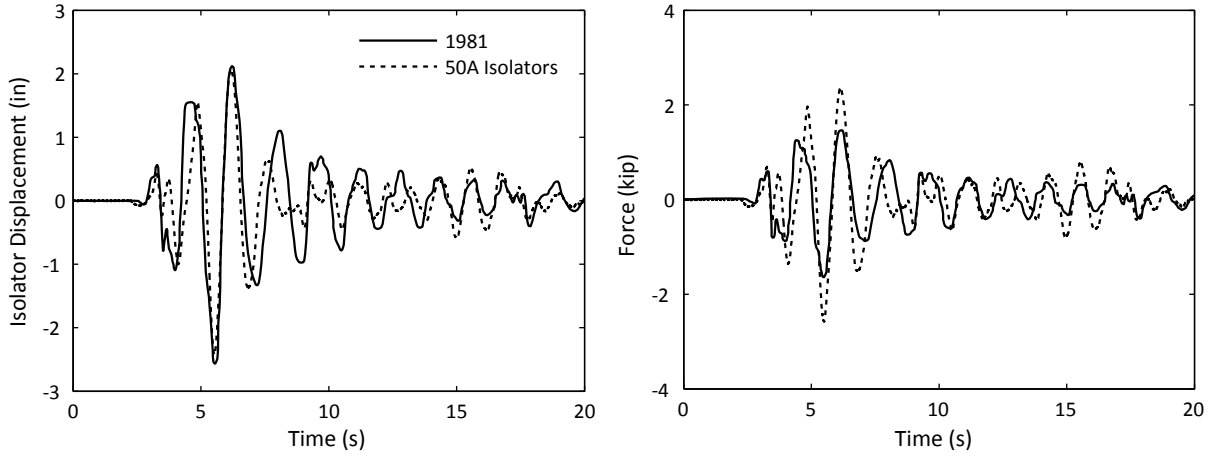

(a) **(b)**

Figure 4.8 Comparison of the Imperial Valley (PGA = 0.543*g*) (a) isolator displacement and (b) mean force time histories presented in Kelly and Hodder [1981] to Imperial Valley Run 5 (PGA = 0.54*g*).

4.1.2.3 Pullback Tests

In the pullback tests conducted by Kelly and Hodder [1981], the dynamic stiffness of the 40A and 50A isolators was 0.50 kip/in. (0.088 kN/mm) and 1.15 kip/in. (0.202 kN/mm), respectively. Table 4.2 shows the percent change of effective horizontal stiffness of the current study for each pullback test to the original study. The effective horizontal stiffness in the current study is obtained from the first full cycle of free vibration. The initial displacement in the original study was about 1 in. (25.4 mm). At this initial displacement the effective horizontal stiffness of the 40A isolator increased between 16% and 68% for the South and Northeast isolator, respectively. The mean increase was 45% and 29% for the 40A and 50A isolators, respectively.

As with the Imperial Valley runs, a general softening trend occurred as the initial displacement increased. Therefore, the percent change shown in Table 4.2 generally decreased with increasing initial displacement, as the effective horizontal stiffness from the original study is constant. The effective horizontal stiffness of the South 40A isolator decreased below the original study at an initial displacement of 1.5 in. (38.1 mm). The mean effective horizontal stiffness of the 50A isolators at an initial displacement of 2.0 in. (50.8 mm) was approximately equal to the original study.

Table 4.2 Percent change of the effective horizontal stiffness obtained from pullback tests.

Initial displacement		40A				50A			
(in.)	(mm)	North	South	Northeast	μ	Northwest	Southeast	Southwest	μ
1.0	25.4	53	16	68	45	24	29	33	29
1.2	30.5	41	5	63	36	21	26	30	26
1.5	38.1	34	2	56	31	15	20	23	19
1.5	38.1	24	-8	44	20	6	13	22	14
1.5	38.1	24	-8	44	20	6	13	22	14
1.5	38.1	22	-10	41	17	3	10	16	10
2.0	50.8	11	-21	32	7	-6	2	5	1

4.2 ISOLATION SYSTEM PERFORMANCE

4.2.1 Pullback Tests

The pullback tests were analyzed by each cycle beginning with the first full cycle after release. The damping was determined utilizing the logarithmic decrement averaged between the decay of the maximum and minimum shear strain over each cycle. The damping in the rigid configuration generally decreased with increasing displacement from 8.3% to 6.3% but was relatively consistent between runs (Figure 4.9a). In the flexible configuration (Figure 4.9b), the variation in damping was increased. Furthermore, the magnitude of the damping also increased with a mean of 8.0% and maximum of 9.1%. The effective horizontal stiffness of the system as a function of

average cycle shear strain is shown in Figure 4.9c and d for the rigid and flexible configuration, respectively. As discussed earlier in this study, a softening trend occurs with increasing displacement.

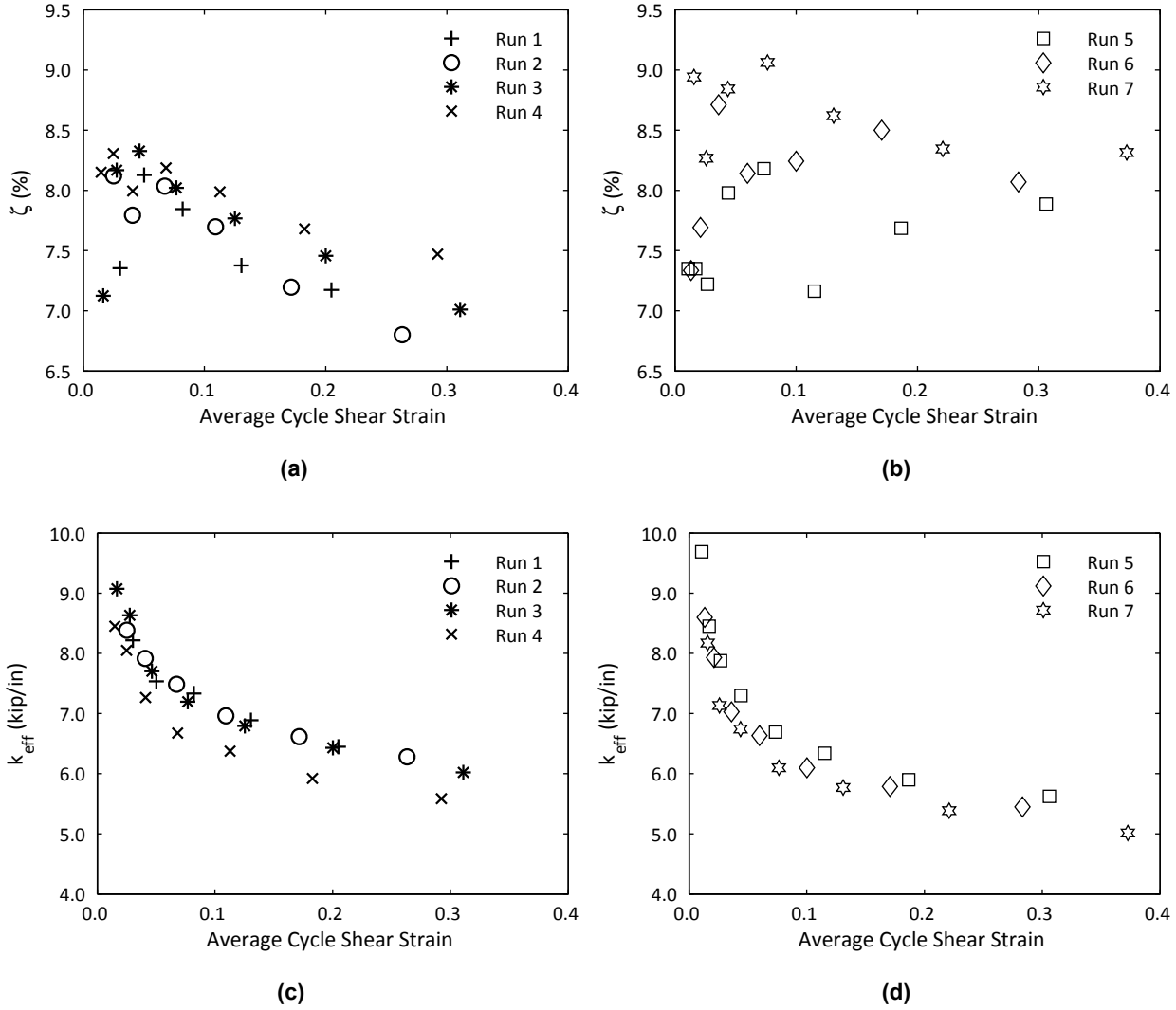

Figure 4.9 **Damping for the (a) rigid and (b) flexible configuration, and the system effective horizontal stiffness for the (c) rigid and (d) flexible configuration as a function of average cycle displacement.**

4.2.2 Historical Earthquakes

4.2.2.1 Time Histories

The shear strain, γ, time histories are shown in Figure 4.10 for each respective earthquake over the time history with the largest peak shear strain of either configuration. An overall maximum shear strain of 1.59 occurred during Loma Prieta Run 13. The maximum shear strain of the other historical earthquakes considered was 1.20, 0.84, and 0.92 for the Imperial Valley, Superstition Hills, and Northridge earthquakes, respectively. As expected, the maximum absolute acceleration of the model structure generally occurred at Level 3 (roof). The magnitude of the absolute

acceleration at Level 1 and 2 was comparable, which is representative of the dominance of the isolation model on the response of the structure. For the largest shear strain runs shown, in all cases the isolation system substantially reduced the absolute acceleration experienced by the model in comparison to the PGA. It is expected that a much larger decrease would be observed if the results were compared to experimental results from an equivalent fixed-base structure. The peak absolute acceleration at Level 3 of the model was 0.17*g*, 0.14*g*, 0.29*g*, and 0.14*g* for the Imperial Valley, Superstition Hills, Loma Prieta, and Northridge earthquakes, respectively, from the runs shown in Figure 4.10.

Figure 4.11 highlights the hysteresis loops of the individual isolators over Imperial Valley Run 7 and Loma Prieta Run 13, which had the two largest peak cycle shear strains of the historical earthquakes. Note that Loma Prieta Run 13 was conducted near the end of the experimental program; the Imperial Valley Run 7, however, was conducted near the beginning of the experimental program (see Appendix A). Similar to the original study, a general softening trend occurred at larger shear strains in addition to a widening of the loops, which is representative of additional energy dissipation. The softening was especially prevalent in the large shear strains of the Loma Prieta cycles. In some cases, such as the Southeast and Northwest 50A isolator and the North 40A isolator, the softening begins to occur earlier than observed in the Imperial Valley run. Review of the vertical force on the individual isolators revealed that the fluctuation in vertical force was larger in Loma Prieta Run 13 than Imperial Valley Run 7. The increased softening observed in the Loma Prieta cycles is in part attributed to the larger fluctuation in vertical force. The maximum vertical force generally coincides at the peak shear strain of any cycle due to the overturning moments. As discussed above, the influence of the vertical force on the Loma Prieta cycles is amplified both due to the larger fluctuation in the magnitude of the vertical force and the larger shear strains that these fluctuations occur at [Nagarajaiah and Ferrell 1999, Buckle et. al 2002]. Although stability is maintained in the 50A isolators, the hysteresis loops of the 40A isolators, specifically the 40A South isolator, is less favorable as the stability limit is approached. The peak cycle hysteresis loops from the respective earthquakes for the individual isolators and the overall isolation system are provided in Appendix B.

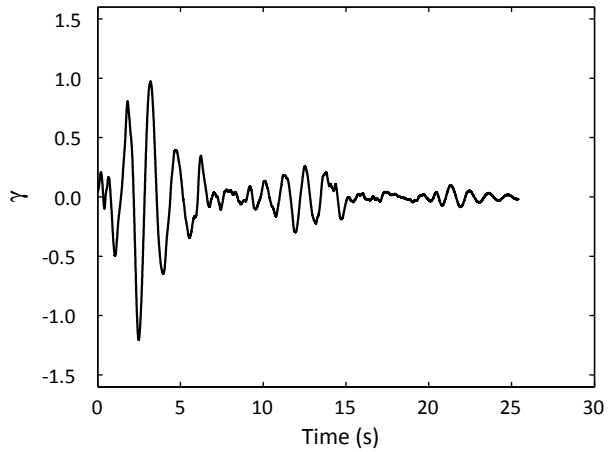

Imperial Valley Run 7 (PGA = 0.67*g*)

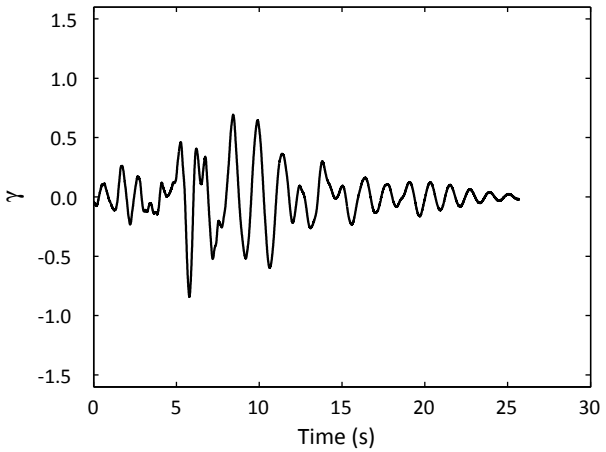

Superstition Hills Run 5 (PGA = 0.6*g*)

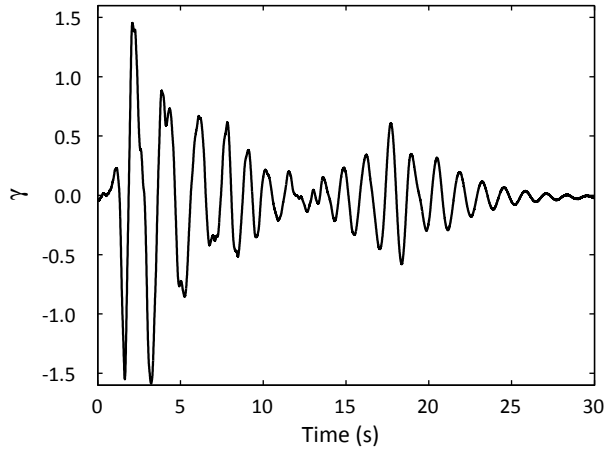

Loma Prieta Run 13 (PGA = 1.16*g*)

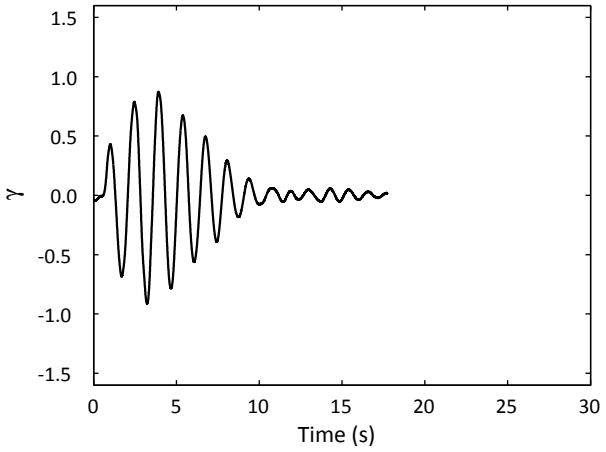

Northridge Run 5 (PGA = 0.29*g*)

Figure 4.10 Historical earthquake shear strain time histories.

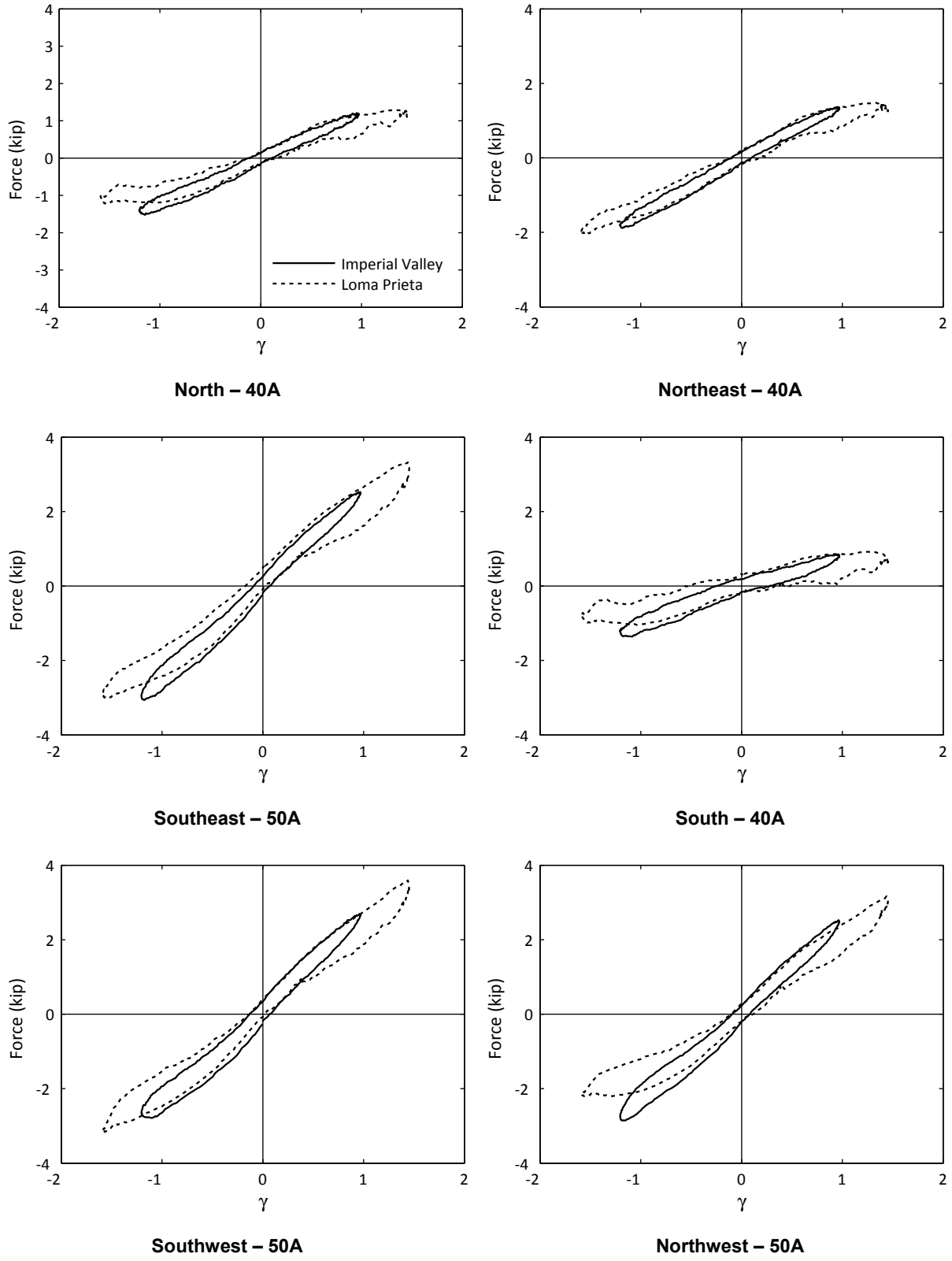

Figure 4.11 Comparison of the individual isolator hysteresis loops from Imperial Valley Run 7 (PGA = 0.67*g*) and Loma Prieta Run 13 (PGA = 1.16*g*).

4.2.2.2 Fundamental Frequency

Figure 4.12 shows the fundamental frequencies for each run determined from the Level 1 accelerations of the structure in the rigid and flexible configuration. The fundamental frequency is plotted as a function of the maximum shear strain recorded over each respective record, γ_{max}. In general, because of the dominance of the isolation mode, the fundamental frequency determined from the acceleration time history at Level 2 and 3 are approximately equal to the fundamental frequency of Level 1. The fundamental frequency generally decreased with increasing maximum shear strain. This is representative of the softening of the system under larger earthquake events. A maximum fundamental frequency of 0.88 Hz was observed in the rigid configuration, corresponding to a full-scale fundamental period of 1.97 sec. The minimum fundamental frequency was 0.56 Hz in the flexible configuration, corresponding to a full-scale fundamental period of 3.09 sec. It is believed that the substantial decrease in fundamental frequency observed in the Loma Prieta runs in the flexible configuration occurred due to the softening at the large shear strain cycles, as discussed earlier.

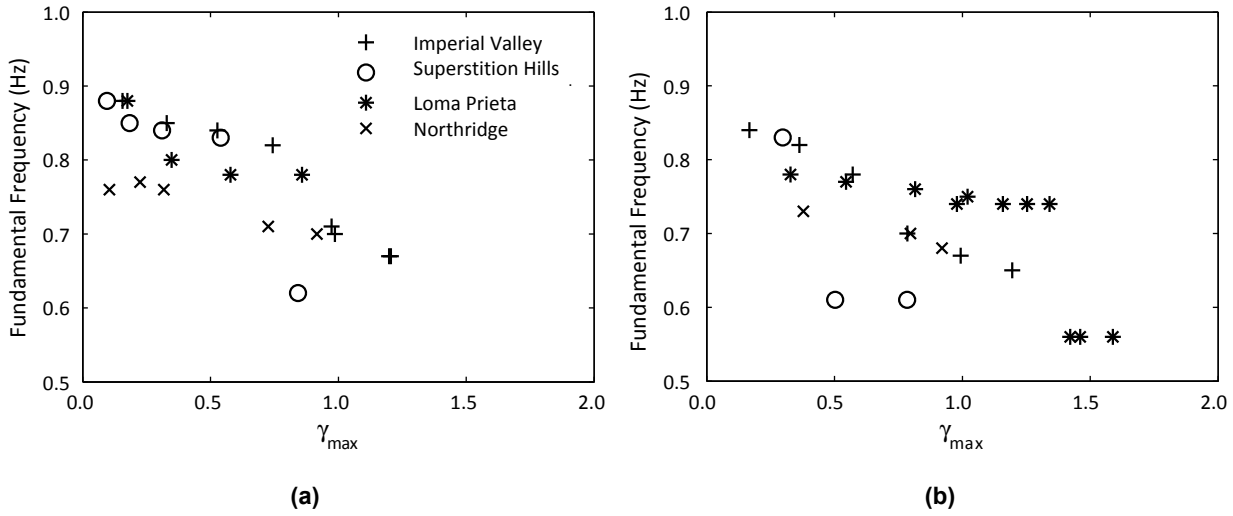

Figure 4.12 Fundamental frequency of the (a) rigid and (b) flexible configuration as a function of maximum shear strain.

4.2.2.3 Peak Cycle Properties

As with the Imperial Valley runs discussed earlier, a general softening trend is observed in the effective horizontal stiffness of the isolation system; see Figure 4.13. A maximum system peak cycle stiffness of 7.24 kip/in. (1.269 kN/mm) was observed in the rigid configuration, and a minimum effective horizontal stiffness of 3.44 kip/in. (0.603 kN/mm) occurred in the flexible configuration. Furthermore, the damping of the system increased with increasing γ_{max}. The large increase in damping at larger values of γ_{max} observed in the Loma Prieta runs in the flexible configuration occurred in part due to the widening of the hysteresis loops over these larger amplitude cycles (see Figure 4.11). In the rigid configuration, the damping ranges between 5.6% and 7.5%, and 5.9% and 8.6% in the flexible configuration.

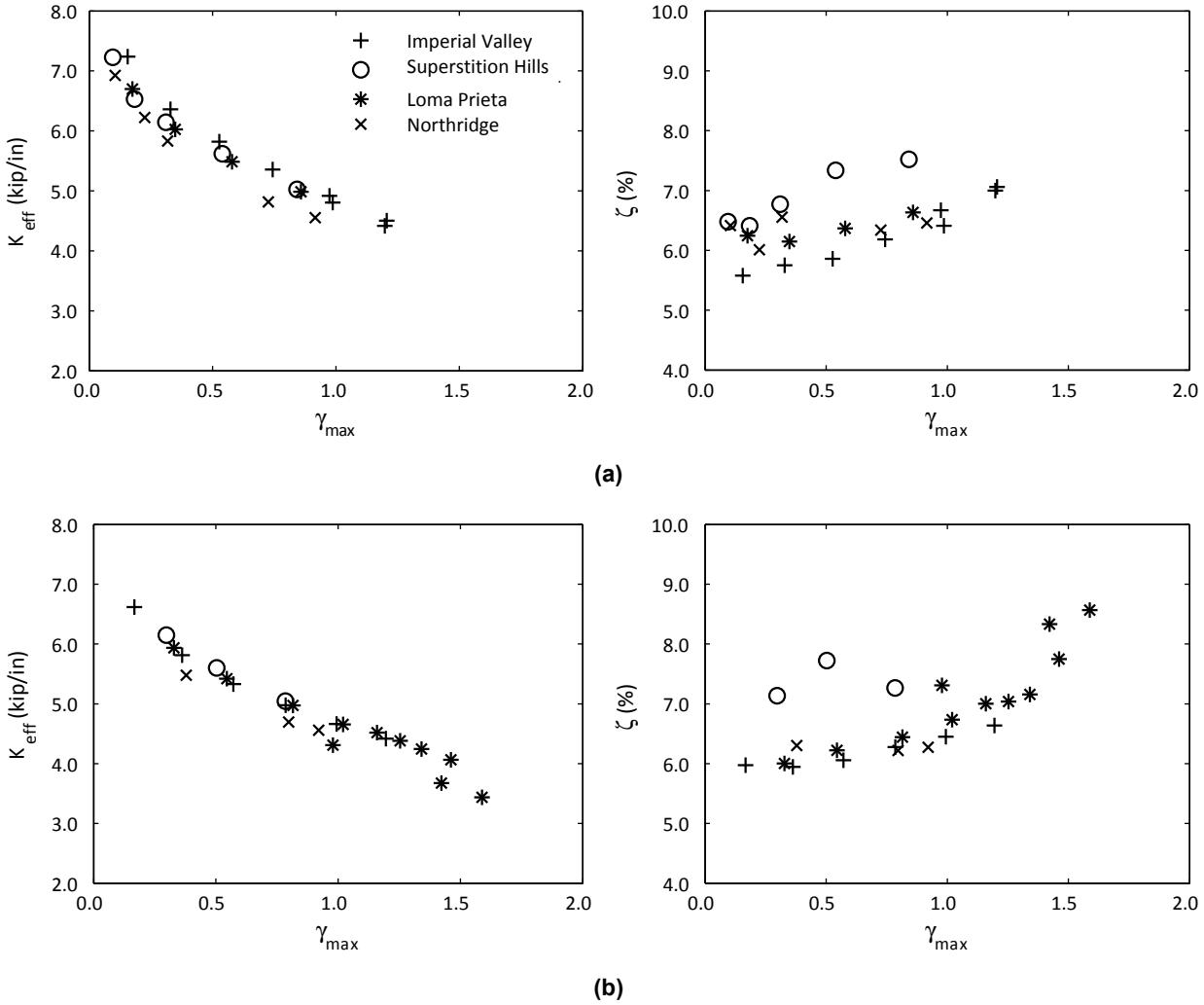

Figure 4.13 Effective horizontal stiffness and equivalent viscous damping for the (a) rigid and (b) flexible configuration as a function of maximum shear strain.

Figure 4.14 displays the collective average stiffness and damping for the 40A and 50A isolators from all historical time histories considered. Results indicate that a high degree of consistency is maintained between the experimental runs with respect to the horizontal stiffness. The average horizontal stiffness of the 40A isolators ranged between 0.35 kip/in. (0.061 kN/mm) and 0.79 kip/in. (0.138 kN/mm), whereas the average effective horizontal stiffness of the 50A isolators ranged between 0.81 kip/in. (0.142 kN/mm) and 1.69 kip/in. (0.296 kN/mm). A larger amount of variation was observed in the damping between the experimental runs. Despite the variation, the mean damping characteristics of the 40A isolators was greater than the 50A isolators, ranging between 6.0% and 12.0%; and 5.3% and 7.7% for the 40A and 50A isolators, respectively.

When investigating the aging characteristics of the isolators, note that the damping of the South 40A isolator was significantly greater than the other 40A isolators. This was observed to be true throughout the experimental program. Figure 4.15 shows the average damping as a function of γ_{max} where the mean damping of the 40A isolators has been determined, omitting the

South 40A isolator. It was found that the damping between the 40A and 50A isolators is comparable with the corrected mean. With omission of the South 40A isolator, the average damping of the 40A isolators ranged between 4.6% and 9.1%, which spans the range of the 50A isolator damping discussed earlier.

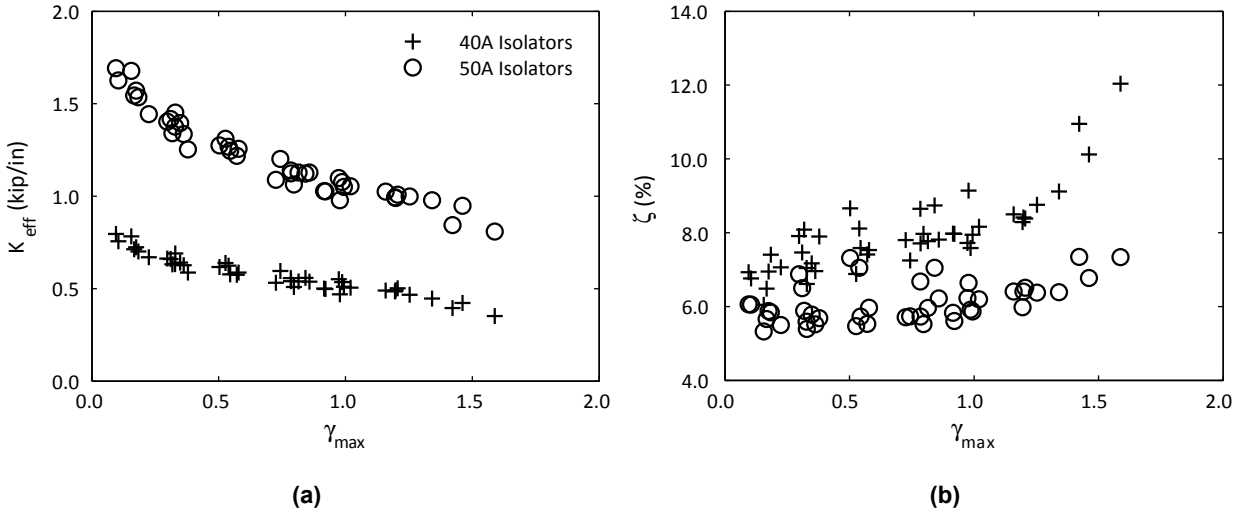

Figure 4.14 Comparison of the mean (a) effective horizontal stiffness and (b) equivalent viscous damping of the 40A and 50A isolators over all historical earthquake runs.

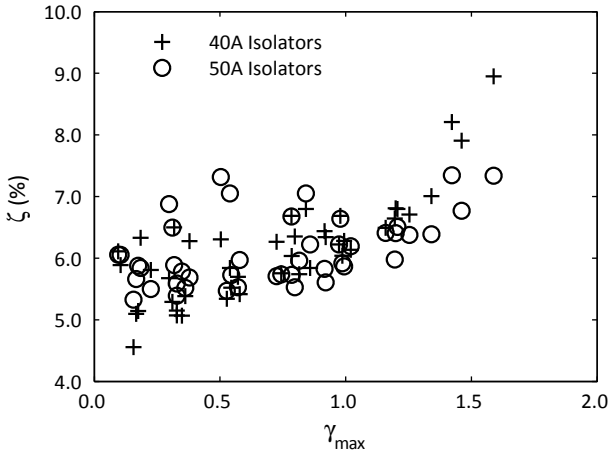

Figure 4.15 Comparison of the mean equivalent viscous damping over all historical earthquake runs omitting the South 40A isolator.

4.2.3 TestQkeIEEE

The *x*-component of the TestQkeIEEE record was the final earthquake time history considered in this study. Unlike the historical earthquake records, the TestQkeIEEE record was not scaled; it

was intended to represent the seismic isolation of sensitive equipment. Furthermore, because of the synthetic nature of the time history, the response spectrum of the TestQkeIEEE is more robust than the historical records considered. Consequently, the response of the isolation system was considerably larger than observed in the historical earthquake time histories. A maximum PGA of 0.20*g* was recorded in TestQkeIEEE Run 4. During this run, the maximum isolator shear strain was 1.69: the largest shear strain recorded in the study. The peak absolute acceleration at Level 3 of the structure was 0.20*g* during this run. The hysteresis loops of the maximum shear strain cycle from TestQkeIEEE Run 4 and Loma Prieta Run 13 for the isolation system are shown in Figure 4.16. Note that good agreement exists between both loops, with a similar consistency observed within each individual isolator.

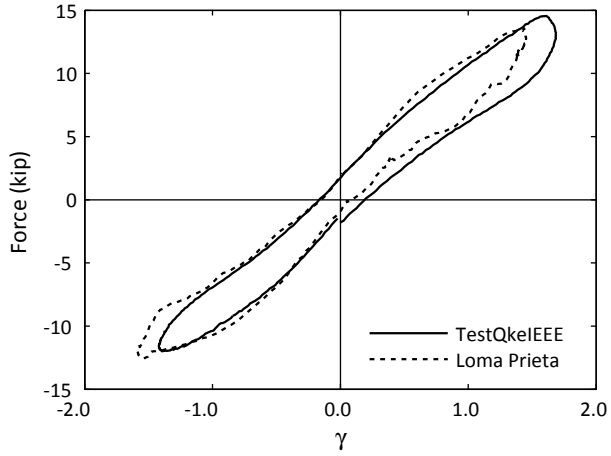

Figure 4.16 Comparison of the isolation system hysteresis loops from TestQkeIEEE Run 4 (PGA = 0.20*g*) and Loma Prieta Run 13 (PGA = 1.16*g*).

5 Discussion

5.1 AGING EFFECTS

The increase in effective horizontal stiffness due to aging was significantly larger than the stiffening observed in other studies of natural or accelerated aging; see Coladant [1993] and Russo et al. [2013]. The increase in effective horizontal stiffness was comparable to the accelerated aging results reported by Yura et al. [2001] for the smaller specimens but observed in a considerably shorter time then predicted for natural aging at ambient temperature. It is postulated that the annular isolators considered in this study were more sensitive to aging due to the increased exposed surface from the unfilled core. If unfilled, the core of an annular isolator is an additional exterior surface that is susceptible to oxidation. Therefore, it is anticipated that an annular isolator would be more sensitive to aging than an identical circular isolator due to a reduced interior region unaffected by the aging process. For the isolators considered, the maximum distance from an exposed edge was 0.88 in. (22.2 mm), which is significantly less than the 2.75 in. (69.9 mm) radius of an identical circular isolator. Therefore, the volume of elastomer protected from oxidation due to the reduced permeability of the oxidized surfaces is considerably reduced.

Note that the average vertical compressive force was 14.5 kip (64.5 kN) per isolator in comparison to 20.0 kip (89.0 kN) in the original study. It is known that the vertical compressive force is inversely proportional to the effective horizontal stiffness and proportional to the damping [Naeim and Kelly 1999]. Therefore, the effective horizontal stiffness is expected to decrease and the damping increase as the vertical compressive force increases. The damping is inversely proportional to the stiffness due to changes in the stored strain energy. Consequently, it is expected that the damping decreases with increasing stiffness.

From Naeim and Kelly [1999], the horizontal stiffness using linear elastic analysis for SREIs is related to the vertical compressive force by:

$$k_h = \frac{GA}{t_r}\left[1 - \left(\frac{P}{P_{crit}}\right)^2\right] \tag{5.1}$$

where k_h is the horizontal stiffness, G is the shear modulus of the elastomer, A is the shear area, t_r is the total thickness of the elastomeric layers, P is the vertical compressive force, and P_{crit} is

the critical load. The compression modulus and bending modulus of a circular and annular pad is reviewed in Appendix C.

The critical loads determined through experimental testing from the original study were 33.4 kip (149 kN) and 53.8 kip (239 kN) for the 40A and 50A isolators, respectively. It is expected that these values would also increase due to the stiffening of the elastomer from aging effects. Using the critical loads from the original study as a reference, from Equation (5.1) the average vertical compressive force of 14.5 kip (64.5 kN) is not negligible, especially for the 40A isolators due to the lower critical load. Furthermore, review of the experimental results shows that the South 40A isolator was overloaded in comparison to the average vertical compressive force, whereas the Southeast and Southwest 50A isolators were approximately equally under-loaded.

The effective horizontal stiffness from the Imperial Valley Run 4 (PGA = 0.45g) hysteresis loop increased by 40 % in the South 40A isolator, which was overloaded, and a mean of 82 % for the remaining two 40A isolators, which were under loaded in comparison to the original study. The large variation observed between the 40A isolators is in part attributed to the discrepancy in the vertical compressive force on the South 40A isolator in contrast to the approximately equally loaded North and Northeast isolators. The range of compressive force on the 40A isolators observed in the experiments brackets the average compressive force in the original study. Consequently, the increase in effective horizontal stiffness due to aging in the 40A isolators is expected to be between 40 % and 82 % if the compressive force between both experimental programs was consistent. The variation in the compressive force and the sensitivity of the 50A isolators to the compressive force was notably lower. Therefore, the increase in effective horizontal stiffness observed is primarily attributed to aging effects; although it is difficult to conclude the exact amount.

5.2 ISOLATOR SYSTEM PERFORMANCE

The fundamental frequency of the model in the original study was 0.5 Hz and 0.75 Hz when isolated with 40A and 50A isolators, respectively [Kelly and Hodder 1981]. The fundamental frequency in the current study ranged between 0.56 Hz and 0.88 Hz determined from the earthquake time histories. A direct comparison between the two studies is difficult due to the different model parameters used in the current study and the combination of testing isolators 40A and 50A simultaneously. Note that increasing the model weight from 80 kip (356 kN) to 87 kip (387 kN) decreases the fundamental frequency, whereas the number of bearings and the increased stiffness of the bearings due to aging effects will increase the fundamental frequency. Despite the change in model parameters and the stiffening of the isolators, the full-scale isolation fundamental period range of 1.97 sec to 3.09 sec is considered sufficient for adequate seismic isolation. A fixed-base fundamental frequency of 2.0 Hz was determined from pullback tests; corresponding to a full scale period of 0.87 sec. Idealizing the structure as a single-degree-of-freedom system and comparing the full-scale spectral acceleration (see Figure 3.5) at the respective fixed-base and base-isolated periods, the overall performance of the base-isolated structure was favorable.

Regardless of the large shear strains, notably in the Loma Prieta and the TestQkeIEEE runs, the isolation system retained stability and favorable seismic isolation characteristics. A maximum shear strain of 1.59 and 1.69 was observed in the historical earthquake records and TestQkeIEEE runs, respectively. This corresponds to a peak displacement normalized by the diameter of the bearing, D, of $D = 0.77$ for TestQkeIEEE Run 4. Figure 5.1 highlights the deformed shape of the bearing at the peak displacement of TestQkeIEEE Run 4, which had a displacement equal to 77% of the diameter. At this level of displacement, the overlap area of the bearing was reduced to approximately 14%. This is a consequence of the unfavorable aspect ratio of the bearing.

There are several main points to be made:

1. Despite a significant increase in horizontal stiffness and related decrease in damping (primarily attributed to aging), the isolation system offered significant protection to the structure.
2. The isolation system was subjected to a large number of earthquakes, many of which constitute beyond design-basis loading. Consistent performance was maintained throughout the program, and the system was able to withstand the repeated large levels of loading.
3. The peak isolator displacements were comparable to those obtained in the original study and are far in excess of what this isolator would be designed for. Even at these extreme displacements and with increased vertical force due to overturning moments, the system remained stable.

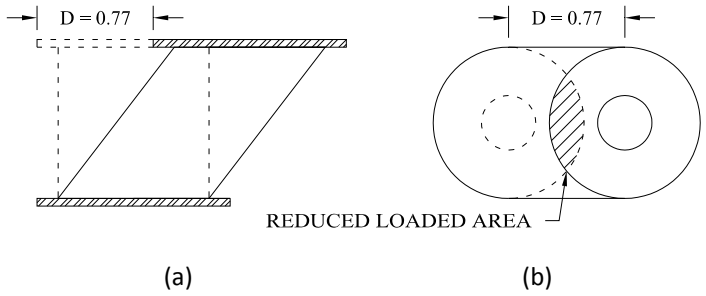

Figure 5.1 Peak displacement (a) profile and (b) plan view of the bearing from the TestQkeIEEE Run 4 highlighting the reduced area.

6 Conclusions

This report investigated the sensitivity of the horizontal properties of Neoprene (Polychloroprene) steel reinforced elastomeric isolators (SREIs) to aging effects. The dynamic behavior of these aged Shore A 40 durometer and 50 durometer isolators was considered up to earthquake inputs that constitute beyond design-basis events. The previously untested annular SREIs were aged unloaded for over 30 years at room temperature. The bearings were compared to the findings of the original experimental program through a series of similar experiments.

It was observed that a significant amount of variation occurred within the horizontal properties of the 40A isolators, whereas the variation within the 50A isolators was within acceptable limits. Peak isolator displacement cycles from the Imperial Valley (1940) El Centro record, considered in both studies, were used to compare the effective horizontal stiffness and equivalent viscous damping. In the current study, both types of isolators exhibited a softening trend as the peak isolator displacement increased. The experimental results were compared by selecting a cycle with approximately equal displacements to the cycles presented in the original study. A significant mean increase in effective horizontal stiffness of 72% and 67% was observed for the 40A and 50A isolators, respectively. Furthermore, with the exception of the South 40A isolator, the equivalent viscous damping decreased by about 50% in all cases. A lower mean increase in effective horizontal stiffness of 45% and 29% for the 40A and 50A isolators, respectively, was observed by comparing the results of the pullback tests of the respective studies.

The increase in stiffness observed in this study was significantly larger, or occurred over a shorter time span, than presented in other studies in the literature on the aging of Neoprene isolation bearings. It was postulated that the unfavorable increase in horizontal stiffness and decrease in damping were amplified due to the unfilled annular design of the isolator, which increases the exposed surface of isolator. Due to the larger ratio of exposed surface to volume, oxidation is able to further penetrate within the elastomer, resulting in a larger volume affected. In addition, it was noted that the vertical compressive force in the current study was less than in the original study. This is also associated with a higher horizontal stiffness. Despite the discrepancy in vertical compressive force, the changes in the properties of the isolators are primarily attributed to aging effects.

The aged performance of Neoprene elastomeric isolators remains an important area for future investigations. The findings in this study indicate that, in spite of considerable changes in aged properties of the isolation bearings, the isolation system retained favorable performance

characteristics. An adequate shift in the fundamental period for seismic isolation was obtained. The system was subjected to a large number of earthquakes, many of which constituted beyond design-basis inputs, and maintained consistent performance throughout the program.

REFERENCES

ASTM International (2010). *Standard Test Method for Rubber – Deterioration by Heat and Oxygen (ASTM D572-04)*, ASTM International, West Conshohocken, PA.

Buckle I., Nagarajaiah S., Ferrell K. (2002). Stability of elastomeric isolation Bearings: experimental study, *J. Struct. Eng.,* 128(1): 3-11.

Burns J., Dubbelday P.S., Ting R.Y. (1990). Dynamic bulk modulus of various elastomers, *J. Polymer Sci. Part B Polymer Phys.,* 28: 1187–1205.

Coladant C. (1993). Durability and aging of elastomeric bearings in Franc, *Proceedings, International Post-SMiRT Conference Seminar*, Ancona, Italy.

Constantinou M.C., Kartoum A., Kelly J.M. (1992). Analysis of compression of hollow circular elastomeric bearings, *Eng. Struct.* 14(2): 103–11.

Fuller K.N.G., Gregory M.J., Harris J.A., Muhr A.H., Roberts A.D., Stevenson A. (1988). Engineering use of natural rubber. In: *Natural Rubber Science and Technology*, A.D. Roberts, ed., New York: Oxford University Press.

ICC-ES (2010). *Acceptance Criteria for Seismic Qualification by Shake-Table Testing of Nonstructural Components and Systems, AC156*, International Code Council Evaluation Service, Inc.

IEEE (2006). *IEEE693: IEEE Recommended Practice for Seismic Design Substations*, Institute of Electrical and Electronic Engineers, Inc., New York, NY.

ISO (2010). *Elastomeric Seismic-Protection Isolators, ISO 22762*, International Organization for Standardization.

Itoh Y., Gu H.-S. (2009). Prediction of aging characteristics in natural rubber bearings used in bridges, *J. Bridge. Eng.* 14(2): 122–128.

Kelly J.M., Hodder S.B. (1981). Experimental study of lead and elastomeric dampers for base isolation systems, *Report No. UCB/EERC 81/16*, Earthquake Engineering Research Center, University of California, Berkeley, CA.

Kelly J.M., Konstantinidis D. (2011). *Mechanics of Rubber Bearings for Seismic Isolation and Vibration Isolation*, Chichester: John Wiley & Sons.

Lindley P.D. (1978). *Engineering Design with Natural Rubber*. NR Technical Bulletin, 4th ed. Brickendonbury, The Malaysian Rubber Producers' Research Association.

Melkumyan M.G. (2011). *New Solutions in Seismic Isolation*, Yerevan: Lusabats Publishing House.

Naeim F., Kelly J.M. (1999). *Design of Seismic Isolated Structural Structures: From Theory to Practice*, New York: John Wiley.

Nagarajaiah S. Ferrell K. (1999). Stability of elastomeric seismic isolation bearings*, J. Struct. Eng.,* 125(9): 946-954.

Russo G., Pauletta M., Cortesia A. (2013). A study on experimental shear behavior of fiber-reinforced elastomeric isolators with various fiber layouts, elastomers, and aging conditions, *Eng. Struct*. 52: 422–433.

Takhirov S.M., Fenves G.L., Fujisaki, E. Clyde, D. (2005). Ground motions for earthquake simulator qualifications of electrical substation equipment, *Report No. PEER 2004/07*, Pacific Earthquake Engineering Research Center, University of California, Berkeley, CA.

Yura J., Kumar A., Yakut A., Topkaya C., Becker E., Collingwood J. (2001). Elastomeric bridge bearings: recommended test methods, *NCHRP Report No. 449*, National Cooperative Highway Research Program, National Academy Press: Washington D.C.

Appendix A Test Sequence

Table A.1 Experimental test sequence.

Seq.	Test	Run	Seq.	Test	Run	Seq.	Test	Run
1	Pullback	1	21	Northridge	5	41	Loma Prieta	7
2	Pullback	2	22	Loma Prieta	1	42	Imperial Valley	14
3	Pullback	3	23	Loma Prieta	2	43	Loma Prieta	8
4	Imperial Valley	1	24	Loma Prieta	3	44	Loma Prieta	9
5	Imperial Valley	2	25	Loma Prieta	4	45	Loma Prieta	10
6	Imperial Valley	3	26	Pullback	4	46	Loma Prieta	11
7	Imperial Valley	4	27	Pullback	5	47	Loma Prieta	12
8	Imperial Valley	5	28	Imperial Valley	9	48	Loma Prieta	13
9	Imperial Valley	6	29	Imperial Valley	10	49	Loma Prieta	14
10	Imperial Valley	7	30	Imperial Valley	11	50	Loma Prieta	15
11	Imperial Valley	8	31	Imperial Valley	12	51	Pullback	6
12	Superstition Hills	1	32	Imperial Valley	13	52	Pullback	7
13	Superstition Hills	2	33	Superstition Hills	6	53	TestQkeIEEE	1
14	Superstition Hills	3	34	Superstition Hills	7	54	TestQkeIEEE	2
15	Superstition Hills	4	35	Superstition Hills	8	55	TestQkeIEEE	3
16	Superstition Hills	5	36	Northridge	6	56	TestQkeIEEE	4
17	Northridge	1	37	Northridge	7	57	TestQkeIEEE	5
18	Northridge	2	38	Northridge	8			
19	Northridge	3	39	Loma Prieta	5			
20	Northridge	4	40	Loma Prieta	6			

Appendix B Peak Cycle Hysteresis Loops

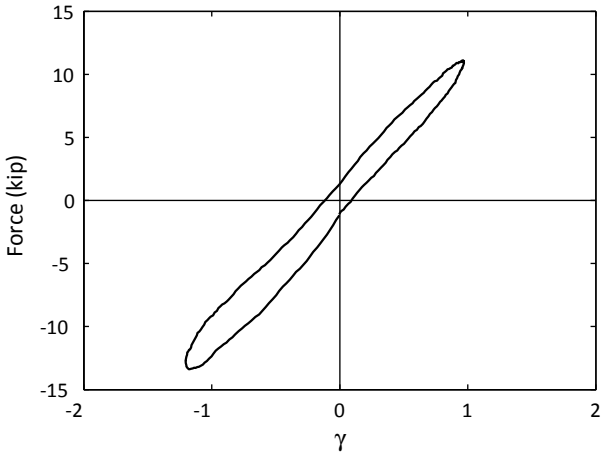

Imperial Valley Run 7 (PGA = 0.67*g*)

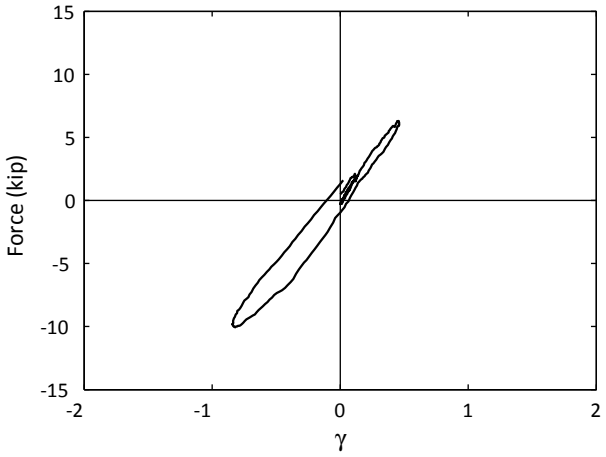

Superstition Hills Run 5 (PGA = 0.60*g*)

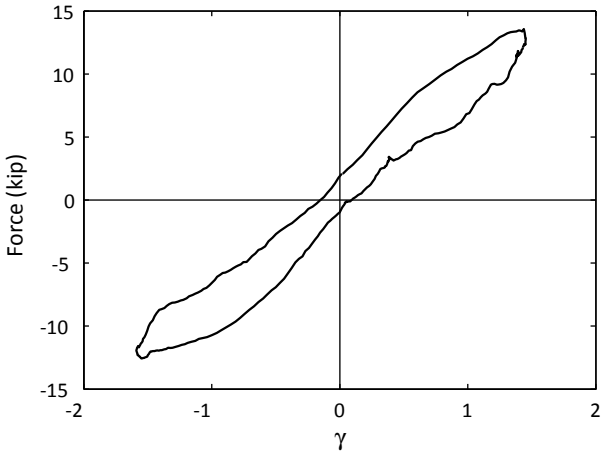

Loma Prieta Run 13 (PGA = 1.16*g*)

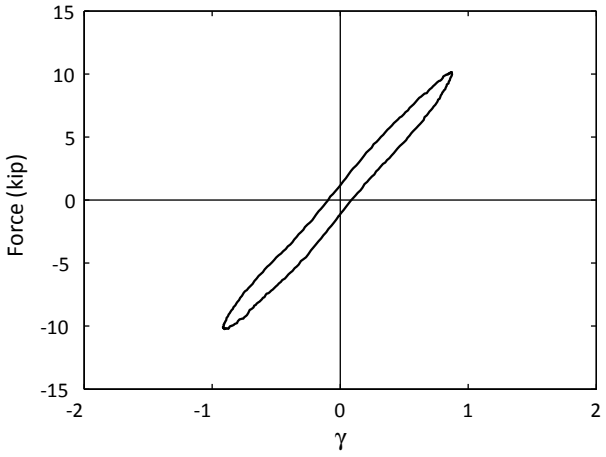

Northridge Run 5 (PGA = 0.29*g*)

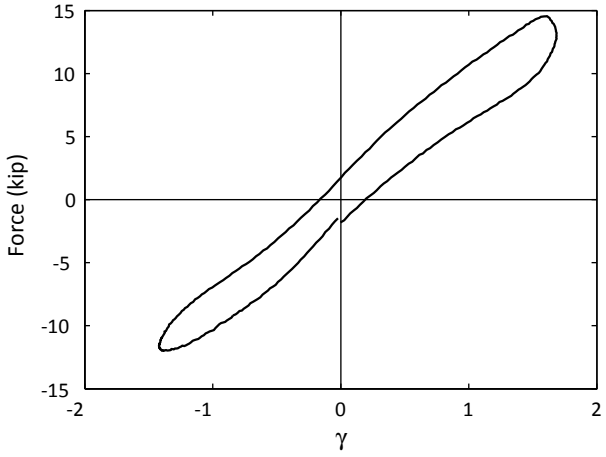

TestQkelEEE Run 4 (PGA = 0.20*g*)

Figure B.1 Peak cycle system hysteresis loops.

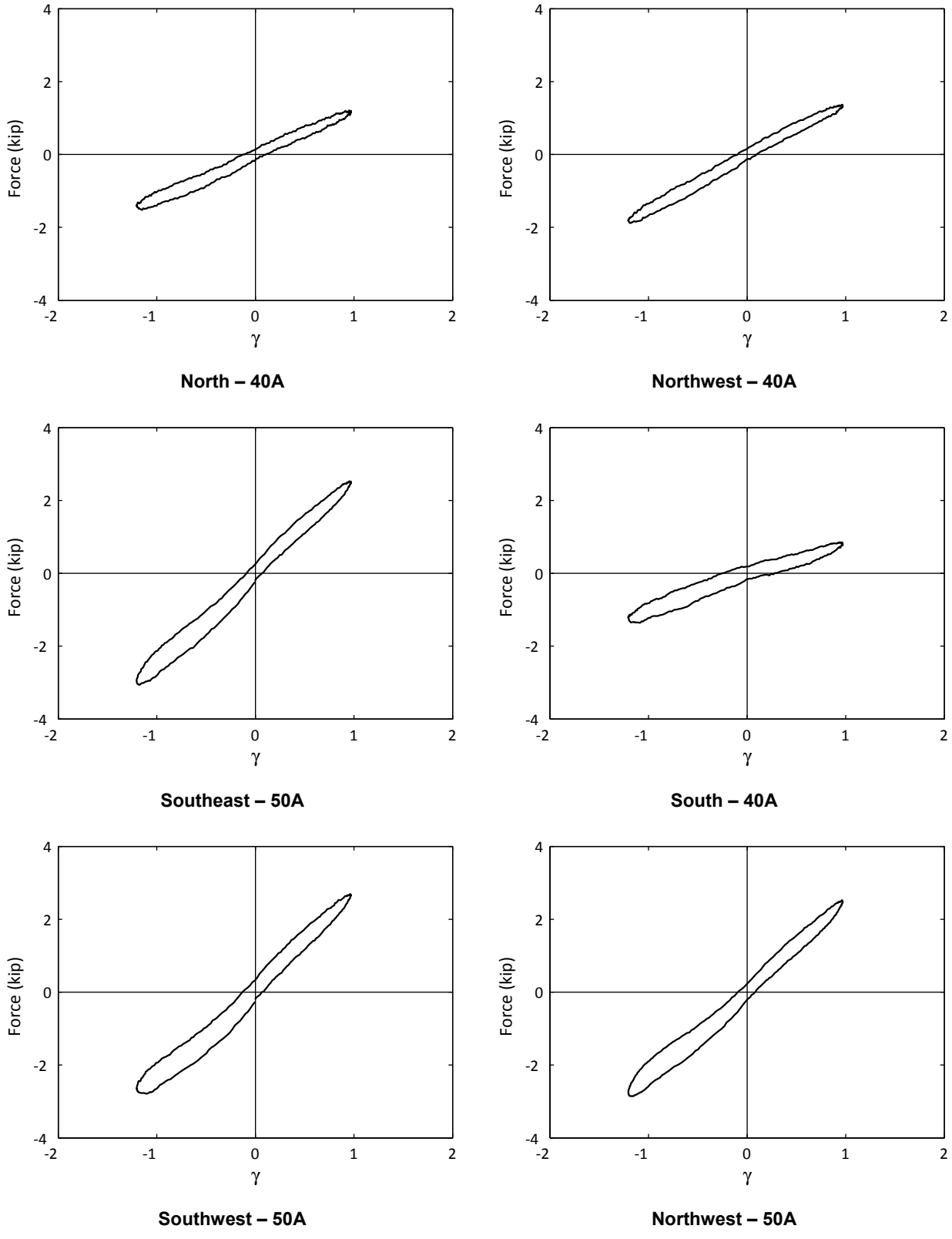

Figure B.2 Imperial Valley Run 7 (PGA = 0.67*g*) peak cycle isolator hysteresis loops.

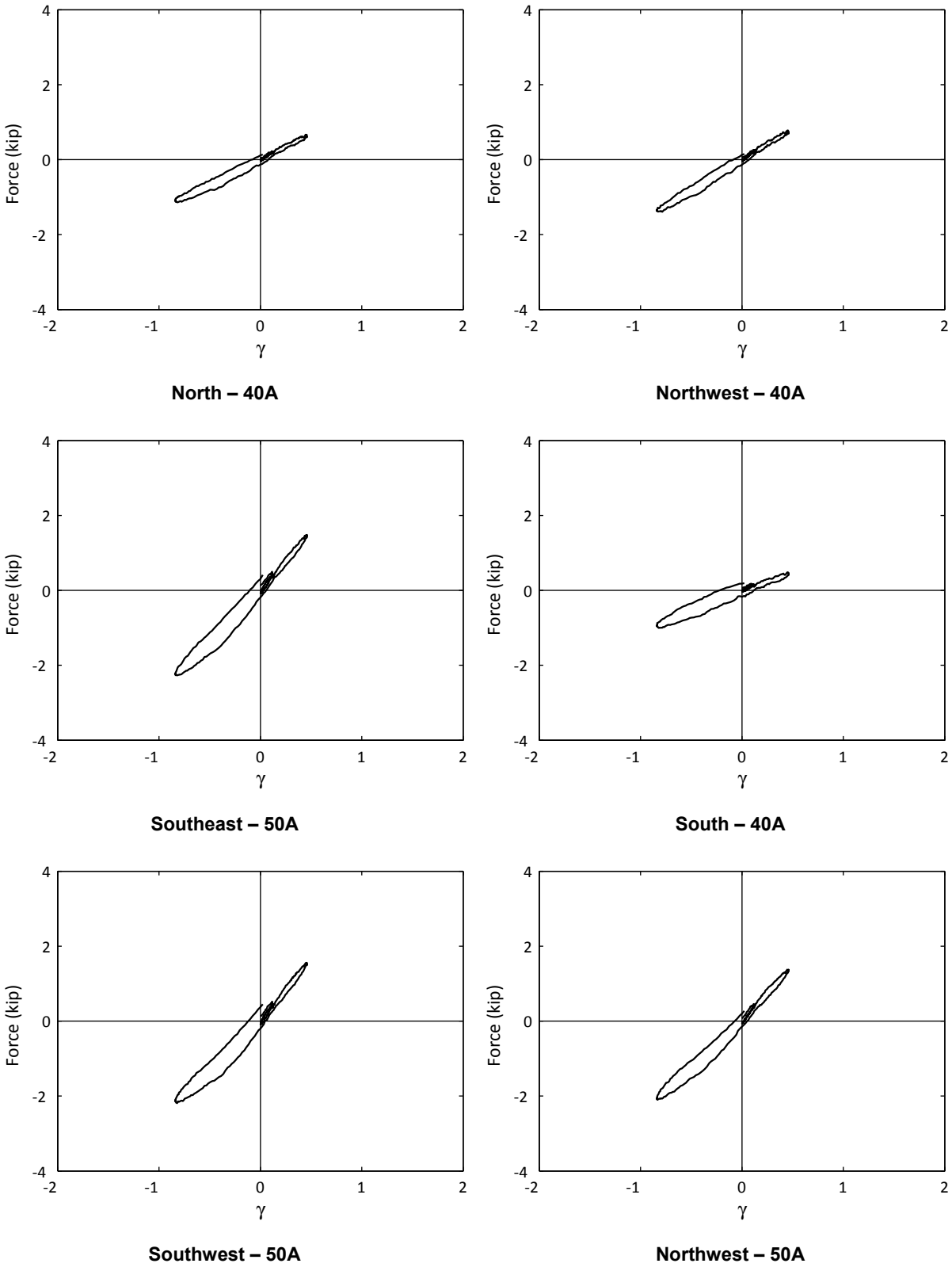

Figure B.3 **Superstition Hills Run 5 (PGA = 0.60*g*) peak cycle isolator hysteresis loops.**

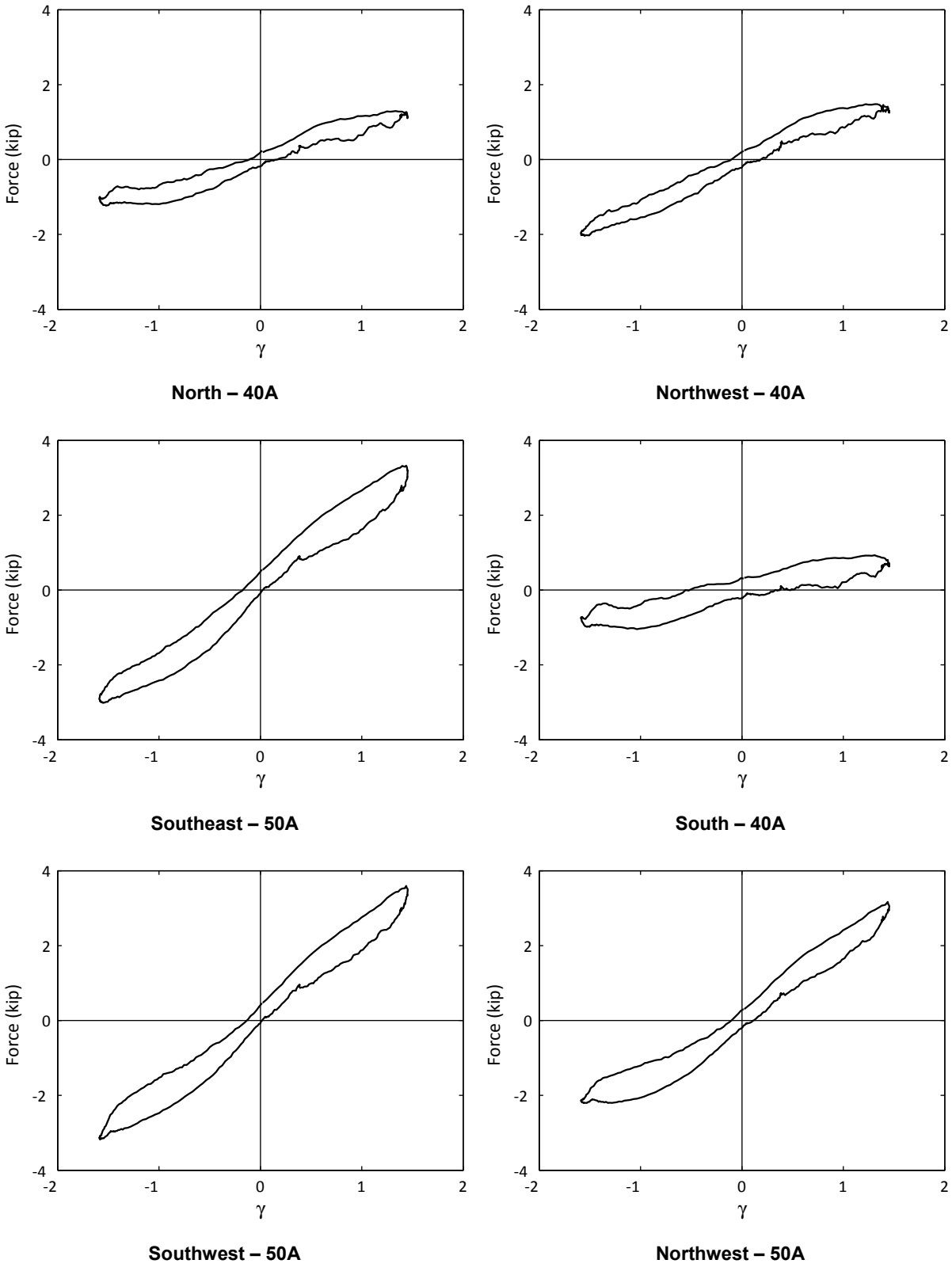

Figure B.4 Loma Prieta Run 13 (PGA = 1.16*g*) peak cycle isolator hysteresis loops.

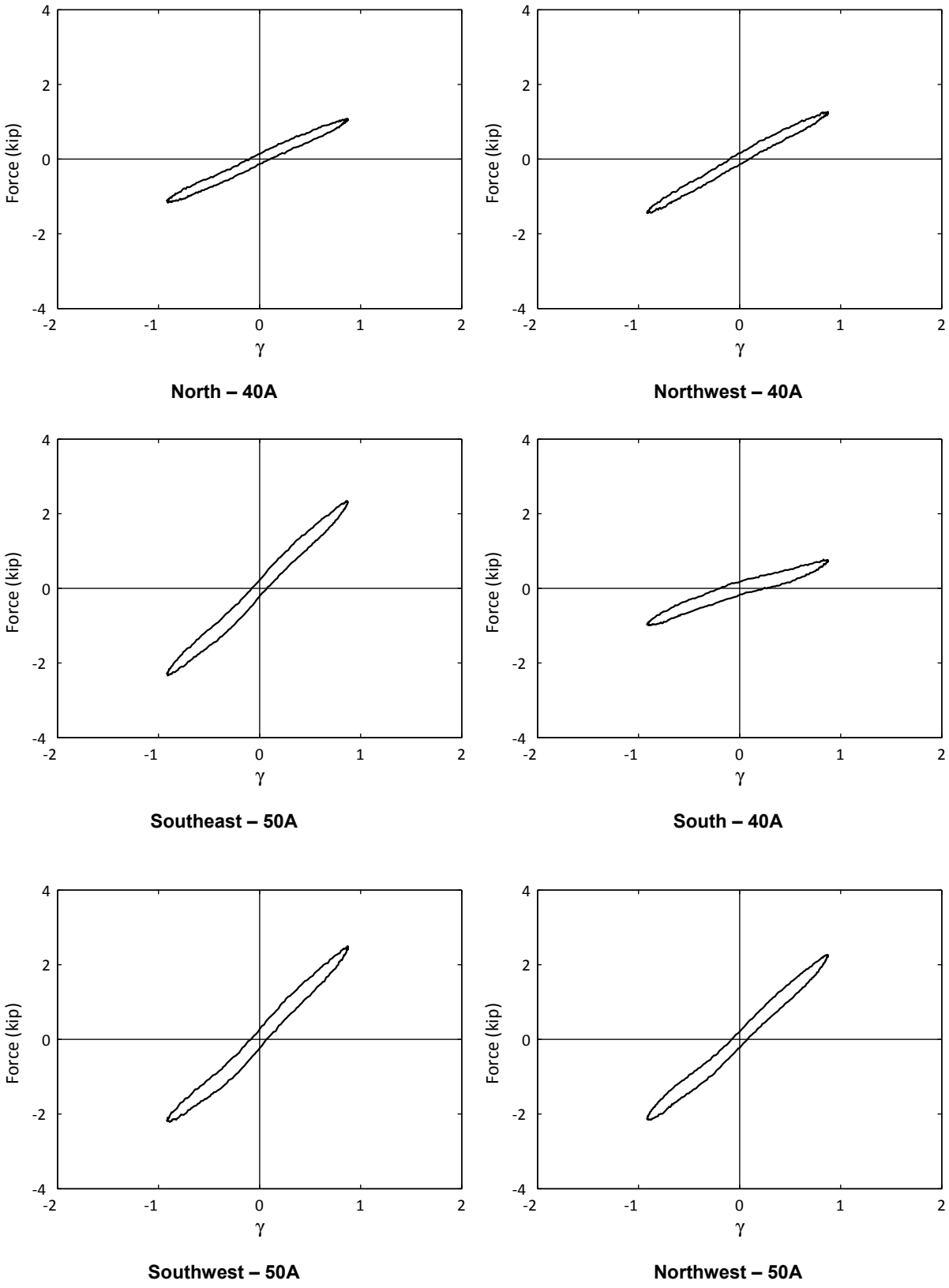

Figure B.5 Northridge Run 5 (PGA = 0.29*g*) peak cycle isolator hysteresis loops.

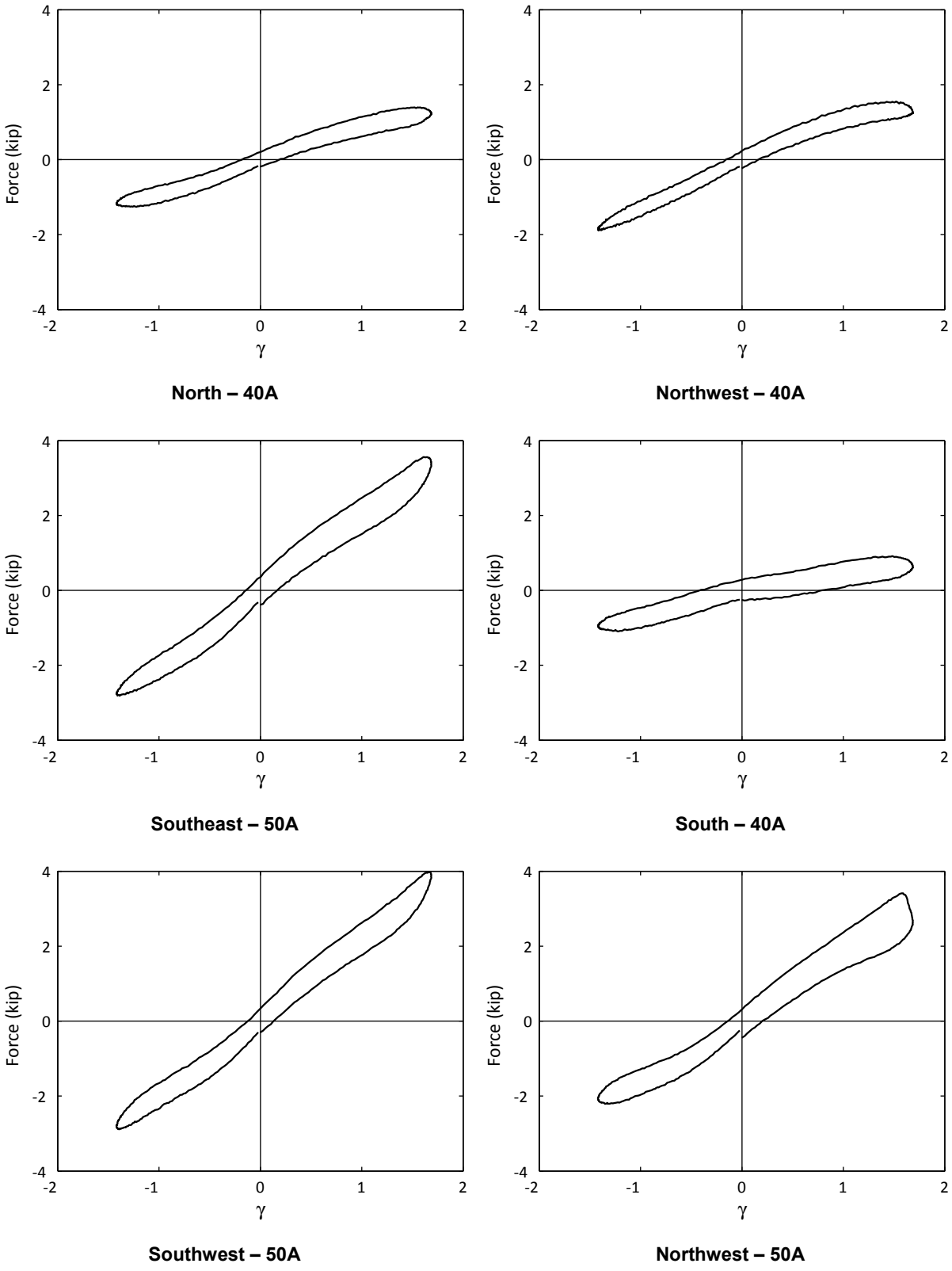

Figure B.6 TestQkelEEE Run 4 (PGA = 0.20*g*) peak cycle isolator hysteresis loops.

Appendix C Mechanical Properties of Circular and Annular Bearings

C.1 COMPRESSION MODULUS

The annular bearing has a number of characteristics that distinguish it from the simpler properties of the fully circular bearing. Consider a single annular pad with an inner radius *a*, outer radius, *b*, and thickness, *t*. The shape factor for this pad is

$$S = \frac{b-a}{2t} \tag{C.1}$$

The material is at first assumed to be incompressible with shear modulus, *G*. The behavior of this pad in pure compression, expressed by the compression modulus, E_c, is given by Constantinou et al. [1992]:

$$E_c = \frac{3G}{2t^2}\left(b^2 + a^2 - \frac{b^2 - a^2}{\ln(b/a)}\right) \tag{C.2}$$

The corresponding solution for the full circular pad is

$$E_c = 6GS^2 \tag{C.3}$$

Therefore, the value of E_c for the annular pad can be expressed as

$$E_c = 6GS^2\lambda \tag{C.4}$$

where

$$\lambda = \frac{b^2 + a^2 - \dfrac{b^2 - a^2}{\ln(b/a)}}{(b-a)^2} \tag{C.5}$$

One of the surprising aspects of this is that the result is very sensitive to the presence of a small hole. In fact, if the size of the hole is greater than 10% of the outer radius, the value of λ is almost two-thirds and the value of E_c is $4GS^2$, which is the solution for an infinite strip.

If the shape factor is large enough, the compression modulus, as computed by the incompressible formula, becomes comparable to the bulk modulus of the compound, and the influence of material compressibility cannot be ignored. The recommended ad hoc modification for compressibility is [ISO 2010]

$$\frac{1}{E_c} = \frac{1}{E_c^{\infty}} + \frac{1}{K} \tag{C.6}$$

where E_c^{∞} is the compression modulus assuming incompressibility, and K is the bulk modulus. This approximation that may not be completely accurate, but the bulk modulus is an extremely difficult quantity to measure, and estimates of the value can vary widely. However, it is somewhat surprising that for quite modest shape factors, the bulk compressibility of the rubber can have an important role for the design formula based on the incompressible model, seriously over-predicting the vertical stiffness and the buckling load of a bearing.

Accordingly, it is essential to have an accurate estimate of the bulk modulus. In particular, a quick review of the data available on this property for natural rubber reveals that an accurate estimate is difficult to find. For example, the widely used handbook *Engineering Design with Natural Rubber*, published by the Malaysian Rubber Producers Research Association (now the Tun Abdul Razac Research Center) [Lindley 1978] provides a table of bulk modulus values based on IRHD hardness that range from 1000 MPa to 1330 MPa as the hardness varies from 30 to 75 IRHD. On the other hand, the reference book *Engineering Use of Natural Rubber*, published by Oxford University Press, gives values in the range 2000 MPa to 3500 MPa [Fuller et al. 1988]. In most applications, the bulk modulus of natural rubber is taken as 2000 MPa. There is even less information on the bulk modulus of Neoprene, but an estimate using a dynamic acoustic wave method by Burns et al. [1990] places it at 3000 MPa.

The exact form of the expression for the compression modulus for a full circular pad is given in Kelly and Konstantinidis [2011] as

$$E_c = K\left(1 - \frac{2}{\lambda R}\frac{I_1(\lambda R)}{I_0(\lambda R)}\right) \tag{C.7}$$

where

$$\lambda^2 R^2 = \frac{48G}{K}S^2 \tag{C.8}$$

and I_0 and I_1 are the zero order and order 1 modified Bessel function of the first kind, respectively.

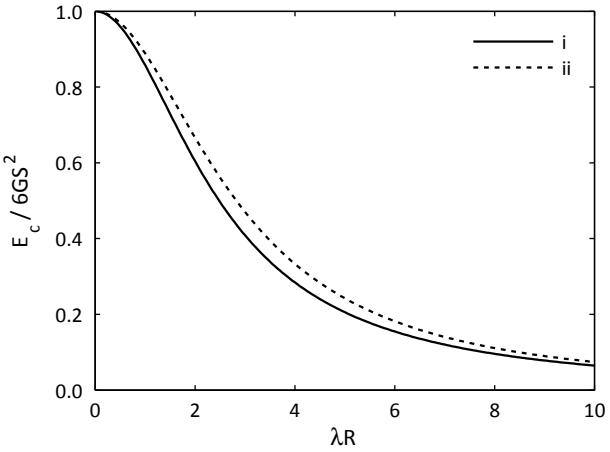

Figure C.1 Comparison of the ratio of the compression modulus with compressible and incompressible rubber for a circular pad.

To compare this result with the *ad hoc* expression, Equations (C.7) and (C.8) are normalize by $6GS^2$ giving for the (i) exact solution

$$\frac{E_c}{6GS^2} = \frac{8}{\lambda^2 R^2}\left(1 - \frac{2}{\lambda R}\frac{I_1(\lambda R)}{I_0(\lambda R)}\right) \tag{C.9}$$

and for the (ii) conventional approximation

$$\frac{E_c}{6GS^2} = \frac{K}{6GS^2 + K} = \frac{1}{1 + \dfrac{\lambda^2 R^2}{8}}$$
$$E_c = K\left\{1 + C_1'\left[I_1(\theta) - \eta I_1(\eta\theta)\right]\right\} + C_2'\left[K_1(\theta) - \eta K_1(\eta\theta)\right] \tag{C.10}$$

Plotting these together in **Error! Reference source not found.** shows that the approximation underestimates the effect of the bulk modulus, but that the error is only about 15%. Considering the uncertainty in the value of K, the use of the simpler form is justified.

For example, if G = 1.0 MPa, K = 2000 MPa, and S = 10, we have 430 MPa for the exact form, while the *ad hoc* formula has 461 MPa. There are two points to be made here: first, the effect of compressibility on the compression modulus happens at a low value of the shape factor; and second, the *ad hoc* solution is not very accurate but is convenient to use.

The exact form of the compression stiffness for the annular pad when compressibility is included is given in Kelly and Konstantinidis [2011] as

$$E_c = K\left\{1 + C_1'\left[I_1(\theta) - \eta I_1(\eta\theta)\right] + C_2'\left[K_1(\theta) - \eta K_1(\eta\theta)\right]\right\} \tag{C.11}$$

where

$$\theta = \sqrt{\frac{48G}{K}}\frac{S}{1-\eta} \tag{C.12}$$

and

$$C_1' = \frac{1}{\sqrt{\frac{12G}{K}}\left(1+\eta S\right)}\,\frac{K_0(\theta)-K_0(\eta\theta)}{I_0(\theta)K_0(\eta\theta)-I_0(\eta\theta)K_0(\theta)} \tag{C.13}$$

$$C_2' = \frac{1}{\sqrt{\frac{12G}{K}}\left(1+\eta S\right)}\,\frac{I_0(\theta)-I_0(\eta\theta)}{I_0(\theta)K_0(\eta\theta)-I_0(\eta\theta)K_0(\theta)} \tag{C.14}$$

with $\eta = a/b$ and where I_0, I_1, and I_0, K_0, K_1 are the order zero and order 1 modified Bessel function of the first and second kind, respectively.

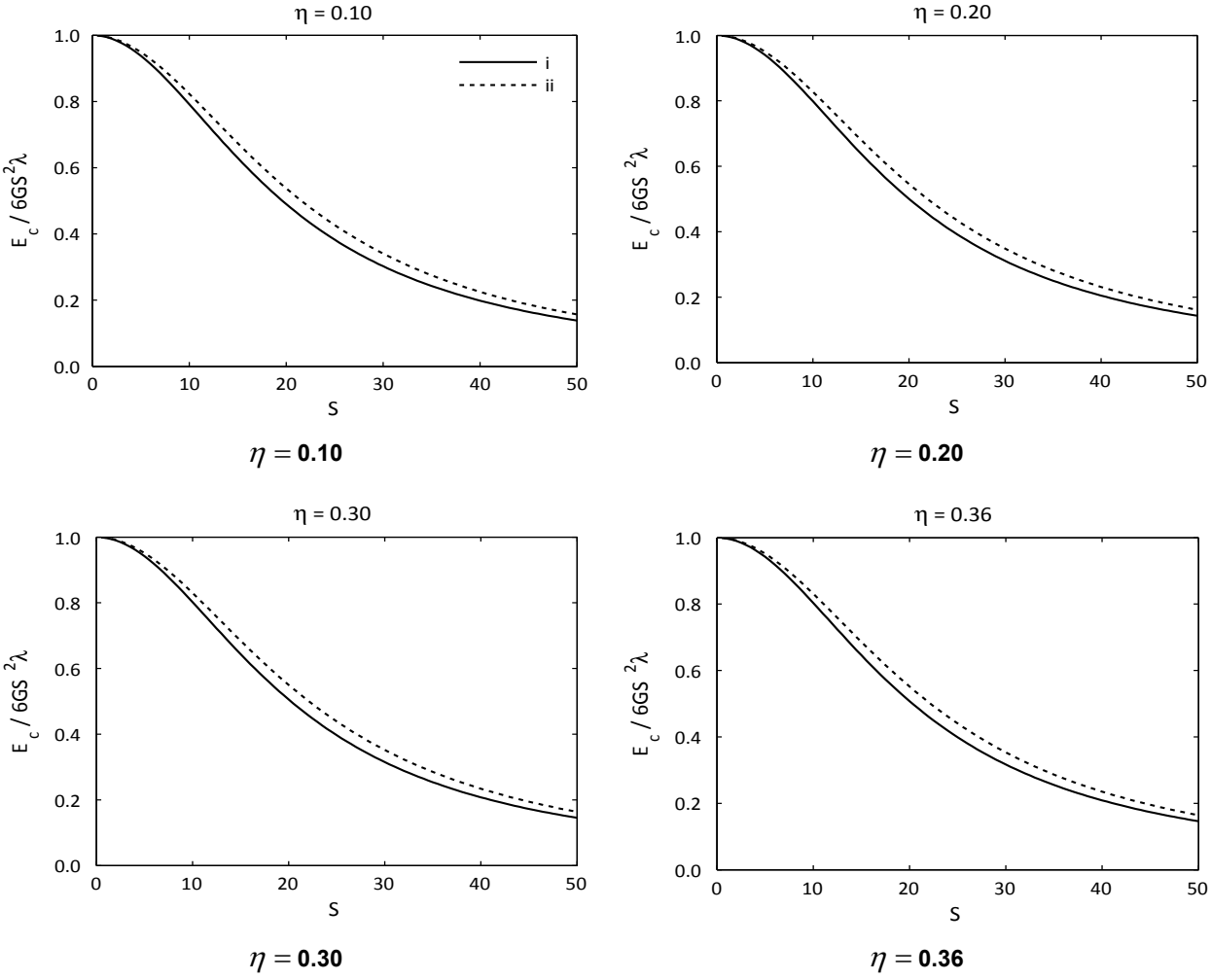

Figure C.2 Comparison of the ratio of the compression modulus with compressible and incompressible rubber for an annular pad.

The (i) exact and (ii) conventional approximation with G = 1.0 MPa, and K = 2000 MPa, are compared in Figure C.2 for annular pads with η = 0.10, 0.20 0.30, and 0.36. The value of η = 0.36 is representative of the annular isolators considered in this study. The maximum error is 13.4% with η = 0.10 and decreases with increasing η. Similar observations can be made as with the circular pad: the effect of compressibility on the compression modulus happens at a low value of shape factor, and that the *ad hoc* solution is not very accurate but is convenient to use.

C.2 BENDING MODULUS

The bending stiffness is required in the computation of the buckling load of a bearing and is denoted by $(EI)_{eff}$. The bending stiffness for a single pad with compressibility included presents a similar problem as with the compression modulus. The conventional approach is to express the effective bending stiffness $(EI)_{eff}$ as $E_b I$, where I is the second moment of area of the pad about an axis perpendicular to the plane of bending and E_b is the bending modulus. To account for bulk compressibility, the bending modulus from the incompressible analysis, E_b^{∞}, is modified using

$$\frac{1}{E_b} = \frac{1}{E_b^{\infty}} + \frac{1}{K} \tag{C.15}$$

This form is recommended in the ISO guidelines [ISO 2010]. The incompressible result for $(EI)_{eff}$ for a full circular pad is

$$(EI)_{eff} = 2GS^2 I = E_c\left(\frac{1}{3}I\right) \tag{C.16}$$

or $E_b = 2GS^2$. The exact form given in Kelly and Konstantinidis [2011] is

$$(EI)_{eff} = \frac{\pi K R^2}{\lambda^2}\left[\frac{\lambda^2 R^2}{4} - \lambda R\frac{I_2(\lambda R)}{I_1(\lambda R)}\right] \tag{C.17}$$

which with $I = \pi R^4/4$ can be written in the form

$$E_b = K\left[1 - \frac{4}{\lambda R}\frac{I_2(\lambda R)}{I_1(\lambda R)}\right] \tag{C.18}$$

Expanding the Bessel Functions in a series for small values of λR gives

$$E_b = 2GS^2\left(1 - \frac{3GS^2}{K}\right) \tag{C.19}$$

which in turn can be inverted and expanded by binomial series to give

$$\frac{1}{E_b} = \frac{1}{2GS^2} + \frac{3}{2K} \tag{C.20}$$

which clearly differs from the conventional approximation. This is viewed as an alternative version of an approximation to the exact form. To compare the exact and the two approximate forms all three are normalized using

$$\lambda^2 R^2 = \frac{48GS^2}{K} \tag{C.21}$$

The three forms are:

(i) exact

$$\frac{E_b}{2GS^2} = \frac{24}{\lambda^2 R^2}\left(1 - \frac{4}{\lambda R}\frac{I_2(\lambda R)}{I_1(\lambda R)}\right) \tag{C.22}$$

(ii) conventional approximation

$$\frac{E_b}{2GS^2} = \frac{1}{1 + \dfrac{\lambda^2 R^2}{24}} \tag{C.23}$$

(iii) new approximation

$$\frac{E_b}{2GS^2} = \frac{1}{1 + \dfrac{\lambda^2 R^2}{16}} \tag{C.24}$$

The comparison of the three forms is shown in Figure C.3a, and the error between the two approximate solutions and the exact solution is shown in Figure C.3b. The error in the conventional approach has a maximum of about 23% at a value of $\lambda R = 7.95$. In contrast, the new approximation is a significant improvement: the maximum error over the range $0 \le \lambda R \le 10$ is 13%. Note that conventional approximation is unconservative, but the new approximation is conservatively lower than the exact solution.

For an annular pad the bending stiffness is given for the incompressible case by

$$(EI)_{eff} = 2GS^2 I \frac{(1+\eta)^2}{(1+\eta^2)} \tag{C.25}$$

where $I = \pi\left(b^4 - a^4\right)/4$ for an annular pad.

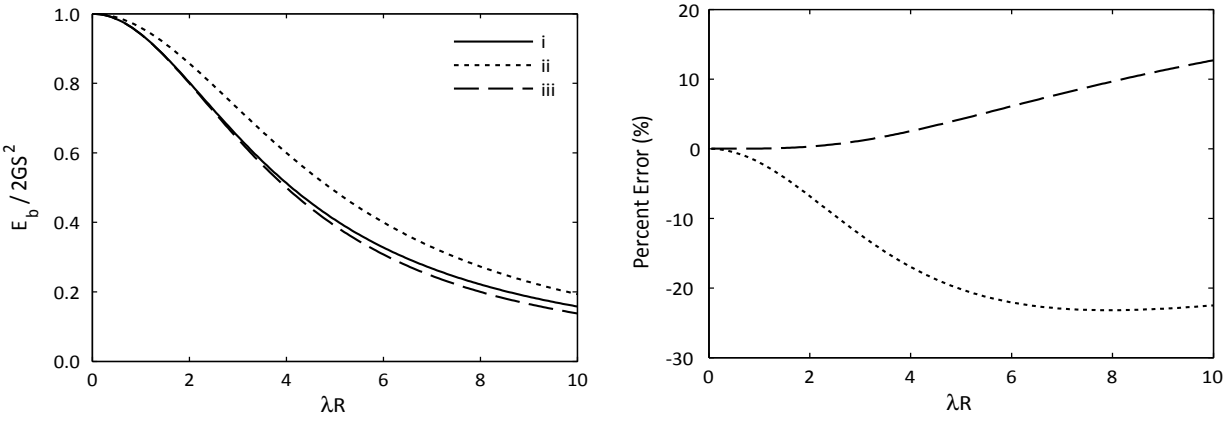

λR λR

(a) **(b)**

Figure C.3 Comparison of the (a) ratio of the effective bending stiffness with compressible rubber to the effective bending stiffness with incompressible rubber; and (b) the associated percent error for a circular pad.

The exact expression for the bending stiffness of an annular pad is given in Kelly and Konstantinidis [2011] as

$$E_b = K\left\{1 - B_1'\left[I_2(\theta) - \eta^2 I_2(\eta\theta)\right] + B_2'\left[K_2(\theta) - \eta^2 K_2(\eta\theta)\right]\right\} \tag{C.26}$$

where

$$B_1' = \frac{4}{\theta\left(1-\eta^4\right)} \frac{-K_1(\eta\theta) + \eta K_1(\theta)}{I_1(\eta\theta)K_1(\theta) - I_1(\theta)K_1(\eta\theta)} \tag{C.27}$$

$$B_2' = \frac{4}{\theta\left(1-\eta^4\right)} \frac{-I_1(\eta\theta) + \eta I_1(\theta)}{I_1(\eta\theta)K_1(\theta) - I_1(\theta)K_1(\eta\theta)} \tag{C.28}$$

and I_2 and K_2 are order 2 modified Bessel functions of the first and second kind, respectively.

The exact expression for the bending stiffness of an annular pad is extremely complicated and really not suitable for design purposes. The recommendation is to use the incompressible result modify it using the conventional approximation

$$\frac{1}{E_b} = \frac{1}{E_b^\infty} + \frac{1}{K} \tag{C.29}$$

or alternatively the new approximation developed for a circular pad

$$\frac{1}{E_b} = \frac{1}{E_b^{\infty}} + \frac{3}{2K} \tag{C.30}$$

The comparison of the (i) exact, (ii) conventional approximation, and (iii) the new approximation with G = 1.0 MPa, and K = 2000 MPa, is shown in Figure C.4, with η = 0.10, 0.20 0.30, and 0.36. The maximum error over the range $0 \le S \le 50$ of the conventional approximation decreases from 18.4% to 15.0% with increasing values of η. Similar to the circular pad, the new approximation offers considerable improvement, with a maximum error of 8.9% to 13.8% at η = 0.10 and 0.36, respectively. Although the difference in the absolute value of the maximum error between the two approximates decreases as η increases, it is important to note that the new approximation provides a conservatively lower value for the bending modulus than the conventional approximation. Furthermore, the value of η is typically small, reducing the error in the new approximation.

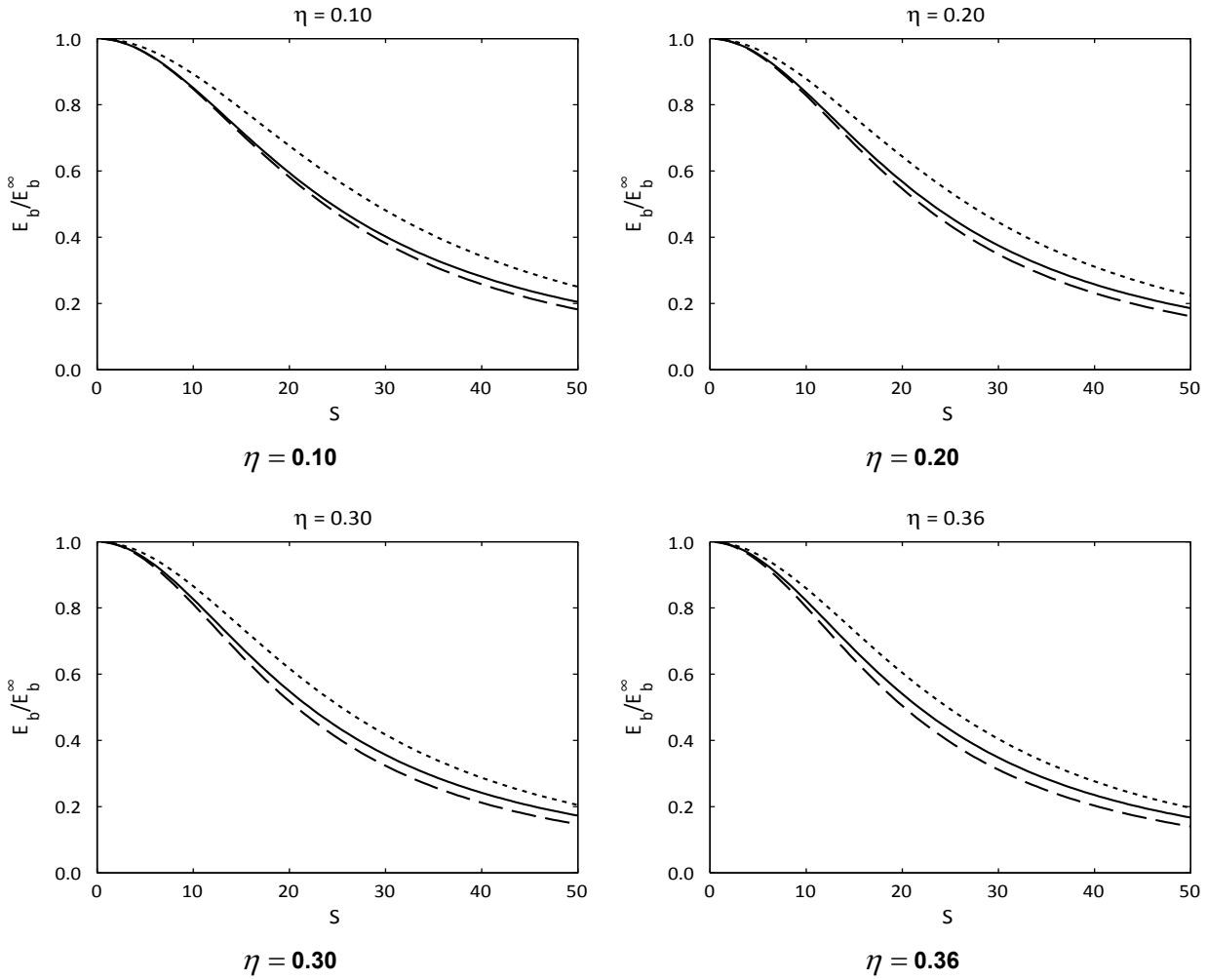

Figure C.4 Comparison of the ratio of the bending modulus with compressible rubber to the effective bending modulus with incompressible rubber for annular pads.

PEER REPORTS

PEER reports are available as a free PDF download from http://peer.berkeley.edu/publications/peer_reports_complete.html. Printed hard copies of PEER reports can be ordered directly from our printer by following the instructions at http://peer.berkeley.edu/publications/peer_reports.html. For other related questions about the PEER Report Series, contact the Pacific Earthquake Engineering Research Center, 325 Davis Hall mail code 1792, Berkeley, CA 94720. Tel.: (510) 642-3437; Fax: (510) 665-1655; Email: peer_editor@berkeley.edu

PEER 2014/03 *Retest of Thirty-Year-Old Neoprene Isolation Bearings.* James M. Kelly and Niel C. Van Engelen. March 2014.

PEER 2014/02 *Theoretical Development of Hybrid Simulation Applied to Plate Structures.* Ahmed A. Bakhaty, Khalid M. Mosalam, and Sanjay Govindjee. January 2014.

PEER 2014/01 *Performance-Based Seismic Assessment of Skewed Bridges.* Peyman Kaviani, Farzin Zareian, and Ertugrul Taciroglu. January 2014.

PEER 2013/25 *Earthquake Engineering for Resilient Communities: 2013 PEER Internship Program Research Report Collection.* Heidi Tremayne (Editor), Stephen A. Mahin (Editor), Jorge Archbold Monterossa, Matt Brosman, Shelly Dean, Katherine deLaveaga, Curtis Fong, Donovan Holder, Rakeeb Khan, Elizabeth Jachens, David Lam, Daniela Martinez Lopez, Mara Minner, Geffen Oren, Julia Pavicic, Melissa Quinonez, Lorena Rodriguez, Sean Salazar, Kelli Slaven, Vivian Steyert, Jenny Taing, and Salvador Tena. December 2013.

PEER 2013/24 *NGA-West2 Ground Motion Prediction Equations for Vertical Ground Motions.* September 2013.

PEER 2013/23 *Coordinated Planning and Preparedness for Fire Following Major Earthquakes.* Charles Scawthorn. November 2013.

PEER 2013/22 *GEM-PEER Task 3 Project: Selection of a Global Set of Ground Motion Prediction Equations.* Jonathan P. Stewart, John Douglas, Mohammad B. Javanbarg, Carola Di Alessandro, Yousef Bozorgnia, Norman A. Abrahamson, David M. Boore, Kenneth W. Campbell, Elise Delavaud, Mustafa Erdik and Peter J. Stafford. December 2013.

PEER 2013/21 *Seismic Design and Performance of Bridges with Columns on Rocking Foundations.* Grigorios Antonellis and Marios Panagiotou. September 2013.

PEER 2013/20 *Experimental and Analytical Studies on the Seismic Behavior of Conventional and Hybrid Braced Frames.* Jiun-Wei Lai and Stephen A. Mahin. September 2013.

PEER 2013/19 *Toward Resilient Communities: A Performance-Based Engineering Framework for Design and Evaluation of the Built Environment.* Michael William Mieler, Bozidar Stojadinovic, Robert J. Budnitz, Stephen A. Mahin and Mary C. Comerio. September 2013.

PEER 2013/18 *Identification of Site Parameters that Improve Predictions of Site Amplification.* Ellen M. Rathje and Sara Navidi. July 2013.

PEER 2013/17 *Response Spectrum Analysis of Concrete Gravity Dams Including Dam-Water-Foundation Interaction.* Arnkjell Løkke and Anil K. Chopra. July 2013.

PEER 2013/16 *Effect of hoop reinforcement spacing on the cyclic response of large reinforced concrete special moment frame beams.* Marios Panagiotou, Tea Visnjic, Grigorios Antonellis, Panagiotis Galanis, and Jack P. Moehle. June 2013.

PEER 2013/15 *A Probabilistic Framework to Include the Effects of Near-Fault Directivity in Seismic Hazard Assessment.* Shrey Kumar Shahi, Jack W. Baker. October 2013.

PEER 2013/14 *Hanging-Wall Scaling using Finite-Fault Simulations.* Jennifer L. Donahue and Norman A. Abrahamson. September 2013.

PEER 2013/13 *Semi-Empirical Nonlinear Site Amplification and its Application in NEHRP Site Factors.* Jonathan P. Stewart and Emel Seyhan. November 2013.

PEER 2013/12 *Nonlinear Horizontal Site Response for the NGA-West2 Project.* Ronnie Kamai, Norman A. Abramson, Walter J. Silva. May 2013.

PEER 2013/11 *Epistemic Uncertainty for NGA-West2 Models.* Linda Al Atik and Robert R. Youngs. May 2013.

PEER 2013/10 *NGA-West 2 Models for Ground-Motion Directionality.* Shrey K. Shahi and Jack W. Baker. May 2013.

PEER 2013/09 *Final Report of the NGA-West2 Directivity Working Group.* Paul Spudich, Jeffrey R. Bayless, Jack W. Baker, Brian S.J. Chiou, Badie Rowshandel, Shrey Shahi, and Paul Somerville. May 2013.

PEER 2013/08 *NGA-West2 Model for Estimating Average Horizontal Values of Pseudo-Absolute Spectral Accelerations Generated by Crustal Earthquakes.* I. M. Idriss. May 2013.

PEER 2013/07 *Update of the Chiou and Youngs NGA Ground Motion Model for Average Horizontal Component of Peak Ground Motion and Response Spectra.* Brian Chiou and Robert Youngs. May 2013.

PEER 2013/06 *NGA-West2 Campbell-Bozorgnia Ground Motion Model for the Horizontal Components of PGA, PGV, and 5%-Damped Elastic Pseudo-Acceleration Response Spectra for Periods Ranging from 0.01 to 10 sec.* Kenneth W. Campbell and Yousef Bozorgnia. May 2013.

PEER 2013/05 *NGA-West 2 Equations for Predicting Response Spectral Accelerations for Shallow Crustal Earthquakes.* David M. Boore, Jonathan P. Stewart, Emel Seyhan, Gail M. Atkinson. May 2013.

PEER 2013/04 *Update of the AS08 Ground-Motion Prediction Equations Based on the NGA-West2 Data Set.* Norman Abrahamson, Walter Silva, and Ronnie Kamai. May 2013.

PEER 2013/03 *PEER NGA-West2 Database.* Timothy D. Ancheta, Robert B. Darragh, Jonathan P. Stewart, Emel Seyhan, Walter J. Silva, Brian S.J. Chiou, Katie E. Wooddell, Robert W. Graves, Albert R. Kottke, David M. Boore, Tadahiro Kishida, and Jennifer L. Donahue. May 2013.

PEER 2013/02 *Hybrid Simulation of the Seismic Response of Squat Reinforced Concrete Shear Walls.* Catherine A. Whyte and Bozidar Stojadinovic. May 2013.

PEER 2013/01 *Housing Recovery in Chile: A Qualitative Mid-program Review.* Mary C. Comerio. February 2013.

PEER 2012/08 *Guidelines for Estimation of Shear Wave Velocity.* Bernard R. Wair, Jason T. DeJong, and Thomas Shantz. December 2012.

PEER 2012/07 *Earthquake Engineering for Resilient Communities: 2012 PEER Internship Program Research Report Collection.* Heidi Tremayne (Editor), Stephen A. Mahin (Editor), Collin Anderson, Dustin Cook, Michael Erceg, Carlos Esparza, Jose Jimenez, Dorian Krausz, Andrew Lo, Stephanie Lopez, Nicole McCurdy, Paul Shipman, Alexander Strum, Eduardo Vega. December 2012.

PEER 2012/06 *Fragilities for Precarious Rocks at Yucca Mountain.* Matthew D. Purvance, Rasool Anooshehpoor, and James N. Brune. December 2012.

PEER 2012/05 *Development of Simplified Analysis Procedure for Piles in Laterally Spreading Layered Soils.* Christopher R. McGann, Pedro Arduino, and Peter Mackenzie–Helnwein. December 2012.

PEER 2012/04 *Unbonded Pre-Tensioned Columns for Bridges in Seismic Regions.* Phillip M. Davis, Todd M. Janes, Marc O. Eberhard, and John F. Stanton. December 2012.

PEER 2012/03 *Experimental and Analytical Studies on Reinforced Concrete Buildings with Seismically Vulnerable Beam-Column Joints.* Sangjoon Park and Khalid M. Mosalam. October 2012.

PEER 2012/02 *Seismic Performance of Reinforced Concrete Bridges Allowed to Uplift during Multi-Directional Excitation.* Andres Oscar Espinoza and Stephen A. Mahin. July 2012.

PEER 2012/01 *Spectral Damping Scaling Factors for Shallow Crustal Earthquakes in Active Tectonic Regions.* Sanaz Rezaeian, Yousef Bozorgnia, I. M. Idriss, Kenneth Campbell, Norman Abrahamson, and Walter Silva. July 2012.

PEER 2011/10 *Earthquake Engineering for Resilient Communities: 2011 PEER Internship Program Research Report Collection.* Eds. Heidi Faison and Stephen A. Mahin. December 2011.

PEER 2011/09 *Calibration of Semi-Stochastic Procedure for Simulating High-Frequency Ground Motions.* Jonathan P. Stewart, Emel Seyhan, and Robert W. Graves. December 2011.

PEER 2011/08 *Water Supply in regard to Fire Following Earthquake.* Charles Scawthorn. November 2011.

PEER 2011/07 *Seismic Risk Management in Urban Areas. Proceedings of a U.S.-Iran-Turkey Seismic Workshop.* September 2011.

PEER 2011/06 *The Use of Base Isolation Systems to Achieve Complex Seismic Performance Objectives.* Troy A. Morgan and Stephen A. Mahin. July 2011.

PEER 2011/05 *Case Studies of the Seismic Performance of Tall Buildings Designed by Alternative Means.* Task 12 Report for the Tall Buildings Initiative. Jack Moehle, Yousef Bozorgnia, Nirmal Jayaram, Pierson Jones, Mohsen Rahnama, Nilesh Shome, Zeynep Tuna, John Wallace, Tony Yang, and Farzin Zareian. July 2011.

PEER 2011/04 *Recommended Design Practice for Pile Foundations in Laterally Spreading Ground.* Scott A. Ashford, Ross W. Boulanger, and Scott J. Brandenberg. June 2011.

PEER 2011/03 *New Ground Motion Selection Procedures and Selected Motions for the PEER Transportation Research Program.* Jack W. Baker, Ting Lin, Shrey K. Shahi, and Nirmal Jayaram. March 2011.

PEER 2011/02 *A Bayesian Network Methodology for Infrastructure Seismic Risk Assessment and Decision Support.* Michelle T. Bensi, Armen Der Kiureghian, and Daniel Straub. March 2011.

PEER 2011/01 *Demand Fragility Surfaces for Bridges in Liquefied and Laterally Spreading Ground.* Scott J. Brandenberg, Jian Zhang, Pirooz Kashighandi, Yili Huo, and Minxing Zhao. March 2011.

PEER 2010/05 *Guidelines for Performance-Based Seismic Design of Tall Buildings.* Developed by the Tall Buildings Initiative. November 2010.

PEER 2010/04 *Application Guide for the Design of Flexible and Rigid Bus Connections between Substation Equipment Subjected to Earthquakes.* Jean-Bernard Dastous and Armen Der Kiureghian. September 2010.

PEER 2010/03 *Shear Wave Velocity as a Statistical Function of Standard Penetration Test Resistance and Vertical Effective Stress at Caltrans Bridge Sites.* Scott J. Brandenberg, Naresh Bellana, and Thomas Shantz. June 2010.

PEER 2010/02 *Stochastic Modeling and Simulation of Ground Motions for Performance-Based Earthquake Engineering.* Sanaz Rezaeian and Armen Der Kiureghian. June 2010.

PEER 2010/01 *Structural Response and Cost Characterization of Bridge Construction Using Seismic Performance Enhancement Strategies.* Ady Aviram, Božidar Stojadinović, Gustavo J. Parra-Montesinos, and Kevin R. Mackie. March 2010.

PEER 2009/03 *The Integration of Experimental and Simulation Data in the Study of Reinforced Concrete Bridge Systems Including Soil-Foundation-Structure Interaction.* Matthew Dryden and Gregory L. Fenves. November 2009.

PEER 2009/02 *Improving Earthquake Mitigation through Innovations and Applications in Seismic Science, Engineering, Communication, and Response. Proceedings of a U.S.-Iran Seismic Workshop.* October 2009.

PEER 2009/01 *Evaluation of Ground Motion Selection and Modification Methods: Predicting Median Interstory Drift Response of Buildings.* Curt B. Haselton, Ed. June 2009.

PEER 2008/10 *Technical Manual for Strata.* Albert R. Kottke and Ellen M. Rathje. February 2009.

PEER 2008/09 *NGA Model for Average Horizontal Component of Peak Ground Motion and Response Spectra.* Brian S.-J. Chiou and Robert R. Youngs. November 2008.

PEER 2008/08 *Toward Earthquake-Resistant Design of Concentrically Braced Steel Structures.* Patxi Uriz and Stephen A. Mahin. November 2008.

PEER 2008/07 *Using OpenSees for Performance-Based Evaluation of Bridges on Liquefiable Soils.* Stephen L. Kramer, Pedro Arduino, and HyungSuk Shin. November 2008.

PEER 2008/06 *Shaking Table Tests and Numerical Investigation of Self-Centering Reinforced Concrete Bridge Columns.* Hyung IL Jeong, Junichi Sakai, and Stephen A. Mahin. September 2008.

PEER 2008/05 *Performance-Based Earthquake Engineering Design Evaluation Procedure for Bridge Foundations Undergoing Liquefaction-Induced Lateral Ground Displacement.* Christian A. Ledezma and Jonathan D. Bray. August 2008.

PEER 2008/04 *Benchmarking of Nonlinear Geotechnical Ground Response Analysis Procedures.* Jonathan P. Stewart, Annie On-Lei Kwok, Yousseff M. A. Hashash, Neven Matasovic, Robert Pyke, Zhiliang Wang, and Zhaohui Yang. August 2008.

PEER 2008/03 *Guidelines for Nonlinear Analysis of Bridge Structures in California.* Ady Aviram, Kevin R. Mackie, and Božidar Stojadinović. August 2008.

PEER 2008/02 *Treatment of Uncertainties in Seismic-Risk Analysis of Transportation Systems.* Evangelos Stergiou and Anne S. Kiremidjian. July 2008.

PEER 2008/01 *Seismic Performance Objectives for Tall Buildings.* William T. Holmes, Charles Kircher, William Petak, and Nabih Youssef. August 2008.

PEER 2007/12 *An Assessment to Benchmark the Seismic Performance of a Code-Conforming Reinforced Concrete Moment-Frame Building.* Curt Haselton, Christine A. Goulet, Judith Mitrani-Reiser, James L. Beck, Gregory G. Deierlein, Keith A. Porter, Jonathan P. Stewart, and Ertugrul Taciroglu. August 2008.

PEER 2007/11 *Bar Buckling in Reinforced Concrete Bridge Columns.* Wayne A. Brown, Dawn E. Lehman, and John F. Stanton. February 2008.

PEER 2007/10 *Computational Modeling of Progressive Collapse in Reinforced Concrete Frame Structures.* Mohamed M. Talaat and Khalid M. Mosalam. May 2008.

PEER 2007/09 *Integrated Probabilistic Performance-Based Evaluation of Benchmark Reinforced Concrete Bridges.* Kevin R. Mackie, John-Michael Wong, and Božidar Stojadinović. January 2008.

PEER 2007/08 *Assessing Seismic Collapse Safety of Modern Reinforced Concrete Moment-Frame Buildings.* Curt B. Haselton and Gregory G. Deierlein. February 2008.

PEER 2007/07 *Performance Modeling Strategies for Modern Reinforced Concrete Bridge Columns.* Michael P. Berry and Marc O. Eberhard. April 2008.

PEER 2007/06 *Development of Improved Procedures for Seismic Design of Buried and Partially Buried Structures.* Linda Al Atik and Nicholas Sitar. June 2007.

PEER 2007/05 *Uncertainty and Correlation in Seismic Risk Assessment of Transportation Systems.* Renee G. Lee and Anne S. Kiremidjian. July 2007.

PEER 2007/04 *Numerical Models for Analysis and Performance-Based Design of Shallow Foundations Subjected to Seismic Loading.* Sivapalan Gajan, Tara C. Hutchinson, Bruce L. Kutter, Prishati Raychowdhury, José A. Ugalde, and Jonathan P. Stewart. May 2008.

PEER 2007/03 *Beam-Column Element Model Calibrated for Predicting Flexural Response Leading to Global Collapse of RC Frame Buildings.* Curt B. Haselton, Abbie B. Liel, Sarah Taylor Lange, and Gregory G. Deierlein. May 2008.

PEER 2007/02 *Campbell-Bozorgnia NGA Ground Motion Relations for the Geometric Mean Horizontal Component of Peak and Spectral Ground Motion Parameters.* Kenneth W. Campbell and Yousef Bozorgnia. May 2007.

PEER 2007/01 *Boore-Atkinson NGA Ground Motion Relations for the Geometric Mean Horizontal Component of Peak and Spectral Ground Motion Parameters.* David M. Boore and Gail M. Atkinson. May. May 2007.

PEER 2006/12 *Societal Implications of Performance-Based Earthquake Engineering.* Peter J. May. May 2007.

PEER 2006/11 *Probabilistic Seismic Demand Analysis Using Advanced Ground Motion Intensity Measures, Attenuation Relationships, and Near-Fault Effects.* Polsak Tothong and C. Allin Cornell. March 2007.

PEER 2006/10 *Application of the PEER PBEE Methodology to the I-880 Viaduct.* Sashi Kunnath. February 2007.

PEER 2006/09 *Quantifying Economic Losses from Travel Forgone Following a Large Metropolitan Earthquake.* James Moore, Sungbin Cho, Yue Yue Fan, and Stuart Werner. November 2006.

PEER 2006/08 *Vector-Valued Ground Motion Intensity Measures for Probabilistic Seismic Demand Analysis.* Jack W. Baker and C. Allin Cornell. October 2006.

PEER 2006/07 *Analytical Modeling of Reinforced Concrete Walls for Predicting Flexural and Coupled–Shear-Flexural Responses.* Kutay Orakcal, Leonardo M. Massone, and John W. Wallace. October 2006.

PEER 2006/06 *Nonlinear Analysis of a Soil-Drilled Pier System under Static and Dynamic Axial Loading.* Gang Wang and Nicholas Sitar. November 2006.

PEER 2006/05 *Advanced Seismic Assessment Guidelines.* Paolo Bazzurro, C. Allin Cornell, Charles Menun, Maziar Motahari, and Nicolas Luco. September 2006.

PEER 2006/04 *Probabilistic Seismic Evaluation of Reinforced Concrete Structural Components and Systems.* Tae Hyung Lee and Khalid M. Mosalam. August 2006.

PEER 2006/03 *Performance of Lifelines Subjected to Lateral Spreading.* Scott A. Ashford and Teerawut Juirnarongrit. July 2006.

PEER 2006/02 *Pacific Earthquake Engineering Research Center Highway Demonstration Project.* Anne Kiremidjian, James Moore, Yue Yue Fan, Nesrin Basoz, Ozgur Yazali, and Meredith Williams. April 2006.

PEER 2006/01 *Bracing Berkeley. A Guide to Seismic Safety on the UC Berkeley Campus.* Mary C. Comerio, Stephen Tobriner, and Ariane Fehrenkamp. January 2006.

PEER 2005/16 *Seismic Response and Reliability of Electrical Substation Equipment and Systems.* Junho Song, Armen Der Kiureghian, and Jerome L. Sackman. April 2006.

PEER 2005/15 *CPT-Based Probabilistic Assessment of Seismic Soil Liquefaction Initiation.* R. E. S. Moss, R. B. Seed, R. E. Kayen, J. P. Stewart, and A. Der Kiureghian. April 2006.

PEER 2005/14 *Workshop on Modeling of Nonlinear Cyclic Load-Deformation Behavior of Shallow Foundations.* Bruce L. Kutter, Geoffrey Martin, Tara Hutchinson, Chad Harden, Sivapalan Gajan, and Justin Phalen. March 2006.

PEER 2005/13 *Stochastic Characterization and Decision Bases under Time-Dependent Aftershock Risk in Performance-Based Earthquake Engineering.* Gee Liek Yeo and C. Allin Cornell. July 2005.

PEER 2005/12 *PEER Testbed Study on a Laboratory Building: Exercising Seismic Performance Assessment.* Mary C. Comerio, editor. November 2005.

PEER 2005/11 *Van Nuys Hotel Building Testbed Report: Exercising Seismic Performance Assessment.* Helmut Krawinkler, editor. October 2005.

PEER 2005/10 *First NEES/E-Defense Workshop on Collapse Simulation of Reinforced Concrete Building Structures.* September 2005.

PEER 2005/09 *Test Applications of Advanced Seismic Assessment Guidelines.* Joe Maffei, Karl Telleen, Danya Mohr, William Holmes, and Yuki Nakayama. August 2006.

PEER 2005/08 *Damage Accumulation in Lightly Confined Reinforced Concrete Bridge Columns.* R. Tyler Ranf, Jared M. Nelson, Zach Price, Marc O. Eberhard, and John F. Stanton. April 2006.

PEER 2005/07 *Experimental and Analytical Studies on the Seismic Response of Freestanding and Anchored Laboratory Equipment.* Dimitrios Konstantinidis and Nicos Makris. January 2005.

PEER 2005/06 *Global Collapse of Frame Structures under Seismic Excitations*. Luis F. Ibarra and Helmut Krawinkler. September 2005.

PEER 2005//05 *Performance Characterization of Bench- and Shelf-Mounted Equipment.* Samit Ray Chaudhuri and Tara C. Hutchinson. May 2006.

PEER 2005/04 *Numerical Modeling of the Nonlinear Cyclic Response of Shallow Foundations.* Chad Harden, Tara Hutchinson, Geoffrey R. Martin, and Bruce L. Kutter. August 2005.

PEER 2005/03 *A Taxonomy of Building Components for Performance-Based Earthquake Engineering.* Keith A. Porter. September 2005.

PEER 2005/02 *Fragility Basis for California Highway Overpass Bridge Seismic Decision Making*. Kevin R. Mackie and Božidar Stojadinović. June 2005.

PEER 2005/01 *Empirical Characterization of Site Conditions on Strong Ground Motion.* Jonathan P. Stewart, Yoojoong Choi, and Robert W. Graves. June 2005.

PEER 2004/09 *Electrical Substation Equipment Interaction: Experimental Rigid Conductor Studies.* Christopher Stearns and André Filiatrault. February 2005.

PEER 2004/08 *Seismic Qualification and Fragility Testing of Line Break 550-kV Disconnect Switches.* Shakhzod M. Takhirov, Gregory L. Fenves, and Eric Fujisaki. January 2005.

PEER 2004/07 *Ground Motions for Earthquake Simulator Qualification of Electrical Substation Equipment.* Shakhzod M. Takhirov, Gregory L. Fenves, Eric Fujisaki, and Don Clyde. January 2005.

PEER 2004/06 *Performance-Based Regulation and Regulatory Regimes.* Peter J. May and Chris Koski. September 2004.

PEER 2004/05 *Performance-Based Seismic Design Concepts and Implementation: Proceedings of an International Workshop.* Peter Fajfar and Helmut Krawinkler, editors. September 2004.

PEER 2004/04 *Seismic Performance of an Instrumented Tilt-up Wall Building.* James C. Anderson and Vitelmo V. Bertero. July 2004.

PEER 2004/03 *Evaluation and Application of Concrete Tilt-up Assessment Methodologies.* Timothy Graf and James O. Malley. October 2004.

PEER 2004/02 *Analytical Investigations of New Methods for Reducing Residual Displacements of Reinforced Concrete Bridge Columns.* Junichi Sakai and Stephen A. Mahin. August 2004.

PEER 2004/01 *Seismic Performance of Masonry Buildings and Design Implications.* Kerri Anne Taeko Tokoro, James C. Anderson, and Vitelmo V. Bertero. February 2004.

PEER 2003/18 *Performance Models for Flexural Damage in Reinforced Concrete Columns.* Michael Berry and Marc Eberhard. August 2003.

PEER 2003/17 *Predicting Earthquake Damage in Older Reinforced Concrete Beam-Column Joints.* Catherine Pagni and Laura Lowes. October 2004.

PEER 2003/16 *Seismic Demands for Performance-Based Design of Bridges.* Kevin Mackie and Božidar Stojadinović. August 2003.

PEER 2003/15 *Seismic Demands for Nondeteriorating Frame Structures and Their Dependence on Ground Motions.* Ricardo Antonio Medina and Helmut Krawinkler. May 2004.

PEER 2003/14 *Finite Element Reliability and Sensitivity Methods for Performance-Based Earthquake Engineering.* Terje Haukaas and Armen Der Kiureghian. April 2004.

PEER 2003/13 *Effects of Connection Hysteretic Degradation on the Seismic Behavior of Steel Moment-Resisting Frames.* Janise E. Rodgers and Stephen A. Mahin. March 2004.

PEER 2003/12 *Implementation Manual for the Seismic Protection of Laboratory Contents: Format and Case Studies.* William T. Holmes and Mary C. Comerio. October 2003.

PEER 2003/11 *Fifth U.S.-Japan Workshop on Performance-Based Earthquake Engineering Methodology for Reinforced Concrete Building Structures.* February 2004.

PEER 2003/10 *A Beam-Column Joint Model for Simulating the Earthquake Response of Reinforced Concrete Frames.* Laura N. Lowes, Nilanjan Mitra, and Arash Altoontash. February 2004.

PEER 2003/09 *Sequencing Repairs after an Earthquake: An Economic Approach.* Marco Casari and Simon J. Wilkie. April 2004.

PEER 2003/08 *A Technical Framework for Probability-Based Demand and Capacity Factor Design (DCFD) Seismic Formats*. Fatemeh Jalayer and C. Allin Cornell. November 2003.

PEER 2003/07 *Uncertainty Specification and Propagation for Loss Estimation Using FOSM Methods.* Jack W. Baker and C. Allin Cornell. September 2003.

PEER 2003/06 *Performance of Circular Reinforced Concrete Bridge Columns under Bidirectional Earthquake Loading*. Mahmoud M. Hachem, Stephen A. Mahin, and Jack P. Moehle. February 2003.

PEER 2003/05 *Response Assessment for Building-Specific Loss Estimation.* Eduardo Miranda and Shahram Taghavi. September 2003.

PEER 2003/04 *Experimental Assessment of Columns with Short Lap Splices Subjected to Cyclic Loads*. Murat Melek, John W. Wallace, and Joel Conte. April 2003.

PEER 2003/03 *Probabilistic Response Assessment for Building-Specific Loss Estimation.* Eduardo Miranda and Hesameddin Aslani. September 2003.

PEER 2003/02 *Software Framework for Collaborative Development of Nonlinear Dynamic Analysis Program.* Jun Peng and Kincho H. Law. September 2003.

PEER 2003/01 *Shake Table Tests and Analytical Studies on the Gravity Load Collapse of Reinforced Concrete Frames.* Kenneth John Elwood and Jack P. Moehle. November 2003.

PEER 2002/24 *Performance of Beam to Column Bridge Joints Subjected to a Large Velocity Pulse.* Natalie Gibson, André Filiatrault, and Scott A. Ashford. April 2002.

PEER 2002/23 *Effects of Large Velocity Pulses on Reinforced Concrete Bridge Columns.* Greg L. Orozco and Scott A. Ashford. April 2002.

PEER 2002/22 *Characterization of Large Velocity Pulses for Laboratory Testing.* Kenneth E. Cox and Scott A. Ashford. April 2002.

PEER 2002/21 *Fourth U.S.-Japan Workshop on Performance-Based Earthquake Engineering Methodology for Reinforced Concrete Building Structures*. December 2002.

PEER 2002/20 *Barriers to Adoption and Implementation of PBEE Innovations.* Peter J. May. August 2002.

PEER 2002/19 *Economic-Engineered Integrated Models for Earthquakes: Socioeconomic Impacts.* Peter Gordon, James E. Moore II, and Harry W. Richardson. July 2002.

PEER 2002/18 *Assessment of Reinforced Concrete Building Exterior Joints with Substandard Details.* Chris P. Pantelides, Jon Hansen, Justin Nadauld, and Lawrence D. Reaveley. May 2002.

PEER 2002/17 *Structural Characterization and Seismic Response Analysis of a Highway Overcrossing Equipped with Elastomeric Bearings and Fluid Dampers: A Case Study.* Nicos Makris and Jian Zhang. November 2002.

PEER 2002/16 *Estimation of Uncertainty in Geotechnical Properties for Performance-Based Earthquake Engineering.* Allen L. Jones, Steven L. Kramer, and Pedro Arduino. December 2002.

PEER 2002/15 *Seismic Behavior of Bridge Columns Subjected to Various Loading Patterns.* Asadollah Esmaeily-Gh. and Yan Xiao. December 2002.

PEER 2002/14 *Inelastic Seismic Response of Extended Pile Shaft Supported Bridge Structures.* T.C. Hutchinson, R.W. Boulanger, Y.H. Chai, and I.M. Idriss. December 2002.

PEER 2002/13 *Probabilistic Models and Fragility Estimates for Bridge Components and Systems.* Paolo Gardoni, Armen Der Kiureghian, and Khalid M. Mosalam. June 2002.

PEER 2002/12 *Effects of Fault Dip and Slip Rake on Near-Source Ground Motions: Why Chi-Chi Was a Relatively Mild M7.6 Earthquake.* Brad T. Aagaard, John F. Hall, and Thomas H. Heaton. December 2002.

PEER 2002/11 *Analytical and Experimental Study of Fiber-Reinforced Strip Isolators*. James M. Kelly and Shakhzod M. Takhirov. September 2002.

PEER 2002/10 *Centrifuge Modeling of Settlement and Lateral Spreading with Comparisons to Numerical Analyses***.** Sivapalan Gajan and Bruce L. Kutter. January 2003.

PEER 2002/09 *Documentation and Analysis of Field Case Histories of Seismic Compression during the 1994 Northridge, California, Earthquake.* Jonathan P. Stewart, Patrick M. Smith, Daniel H. Whang, and Jonathan D. Bray. October 2002.

PEER 2002/08 *Component Testing, Stability Analysis and Characterization of Buckling-Restrained Unbonded Braces™.* Cameron Black, Nicos Makris, and Ian Aiken. September 2002.

PEER 2002/07 *Seismic Performance of Pile-Wharf Connections.* Charles W. Roeder, Robert Graff, Jennifer Soderstrom, and Jun Han Yoo. December 2001.

PEER 2002/06 *The Use of Benefit-Cost Analysis for Evaluation of Performance-Based Earthquake Engineering Decisions*. Richard O. Zerbe and Anthony Falit-Baiamonte. September 2001.

PEER 2002/05 *Guidelines, Specifications, and Seismic Performance Characterization of Nonstructural Building Components and Equipment*. André Filiatrault, Constantin Christopoulos, and Christopher Stearns. September 2001.

PEER 2002/04 *Consortium of Organizations for Strong-Motion Observation Systems and the Pacific Earthquake Engineering Research Center Lifelines Program: Invited Workshop on Archiving and Web Dissemination of Geotechnical Data, 4–5 October 2001*. September 2002.

PEER 2002/03 *Investigation of Sensitivity of Building Loss Estimates to Major Uncertain Variables for the Van Nuys Testbed.* Keith A. Porter, James L. Beck, and Rustem V. Shaikhutdinov. August 2002.

PEER 2002/02 *The Third U.S.-Japan Workshop on Performance-Based Earthquake Engineering Methodology for Reinforced Concrete Building Structures*. July 2002.

PEER 2002/01 *Nonstructural Loss Estimation: The UC Berkeley Case Study.* Mary C. Comerio and John C. Stallmeyer. December 2001.

PEER 2001/16 *Statistics of SDF-System Estimate of Roof Displacement for Pushover Analysis of Buildings.* Anil K. Chopra, Rakesh K. Goel, and Chatpan Chintanapakdee. December 2001.

PEER 2001/15 *Damage to Bridges during the 2001 Nisqually Earthquake.* R. Tyler Ranf, Marc O. Eberhard, and Michael P. Berry. November 2001.

PEER 2001/14 *Rocking Response of Equipment Anchored to a Base Foundation.* Nicos Makris and Cameron J. Black. September 2001.

PEER 2001/13 *Modeling Soil Liquefaction Hazards for Performance-Based Earthquake Engineering.* Steven L. Kramer and Ahmed-W. Elgamal. February 2001.

PEER 2001/12 *Development of Geotechnical Capabilities in OpenSees.* Boris Jeremić. September 2001.

PEER 2001/11 *Analytical and Experimental Study of Fiber-Reinforced Elastomeric Isolators*. James M. Kelly and Shakhzod M. Takhirov. September 2001.

PEER 2001/10 *Amplification Factors for Spectral Acceleration in Active Regions.* Jonathan P. Stewart, Andrew H. Liu, Yoojoong Choi, and Mehmet B. Baturay. December 2001.

PEER 2001/09 *Ground Motion Evaluation Procedures for Performance-Based Design.* Jonathan P. Stewart, Shyh-Jeng Chiou, Jonathan D. Bray, Robert W. Graves, Paul G. Somerville, and Norman A. Abrahamson. September 2001.

PEER 2001/08 *Experimental and Computational Evaluation of Reinforced Concrete Bridge Beam-Column Connections for Seismic Performance*. Clay J. Naito, Jack P. Moehle, and Khalid M. Mosalam. November 2001.

PEER 2001/07 *The Rocking Spectrum and the Shortcomings of Design Guidelines.* Nicos Makris and Dimitrios Konstantinidis. August 2001.

PEER 2001/06 *Development of an Electrical Substation Equipment Performance Database for Evaluation of Equipment Fragilities*. Thalia Agnanos. April 1999.

PEER 2001/05 *Stiffness Analysis of Fiber-Reinforced Elastomeric Isolators.* Hsiang-Chuan Tsai and James M. Kelly. May 2001.

PEER 2001/04 *Organizational and Societal Considerations for Performance-Based Earthquake Engineering.* Peter J. May. April 2001.

PEER 2001/03 *A Modal Pushover Analysis Procedure to Estimate Seismic Demands for Buildings: Theory and Preliminary Evaluation.* Anil K. Chopra and Rakesh K. Goel. January 2001.

PEER 2001/02 *Seismic Response Analysis of Highway Overcrossings Including Soil-Structure Interaction.* Jian Zhang and Nicos Makris. March 2001.

PEER 2001/01 *Experimental Study of Large Seismic Steel Beam-to-Column Connections.* Egor P. Popov and Shakhzod M. Takhirov. November 2000.

PEER 2000/10 *The Second U.S.-Japan Workshop on Performance-Based Earthquake Engineering Methodology for Reinforced Concrete Building Structures.* March 2000.

PEER 2000/09 *Structural Engineering Reconnaissance of the August 17, 1999 Earthquake: Kocaeli (Izmit), Turkey.* Halil Sezen, Kenneth J. Elwood, Andrew S. Whittaker, Khalid Mosalam, John J. Wallace, and John F. Stanton. December 2000.

PEER 2000/08 *Behavior of Reinforced Concrete Bridge Columns Having Varying Aspect Ratios and Varying Lengths of Confinement.* Anthony J. Calderone, Dawn E. Lehman, and Jack P. Moehle. January 2001.

PEER 2000/07 *Cover-Plate and Flange-Plate Reinforced Steel Moment-Resisting Connections.* Taejin Kim, Andrew S. Whittaker, Amir S. Gilani, Vitelmo V. Bertero, and Shakhzod M. Takhirov. September 2000.

PEER 2000/06 *Seismic Evaluation and Analysis of 230-kV Disconnect Switches.* Amir S. J. Gilani, Andrew S. Whittaker, Gregory L. Fenves, Chun-Hao Chen, Henry Ho, and Eric Fujisaki. July 2000.

PEER 2000/05 *Performance-Based Evaluation of Exterior Reinforced Concrete Building Joints for Seismic Excitation.* Chandra Clyde, Chris P. Pantelides, and Lawrence D. Reaveley. July 2000.

PEER 2000/04 *An Evaluation of Seismic Energy Demand: An Attenuation Approach.* Chung-Che Chou and Chia-Ming Uang. July 1999.

PEER 2000/03 *Framing Earthquake Retrofitting Decisions: The Case of Hillside Homes in Los Angeles.* Detlof von Winterfeldt, Nels Roselund, and Alicia Kitsuse. March 2000.

PEER 2000/02 *U.S.-Japan Workshop on the Effects of Near-Field Earthquake Shaking.* Andrew Whittaker, ed. July 2000.

PEER 2000/01 *Further Studies on Seismic Interaction in Interconnected Electrical Substation Equipment.* Armen Der Kiureghian, Kee-Jeung Hong, and Jerome L. Sackman. November 1999.

PEER 1999/14 *Seismic Evaluation and Retrofit of 230-kV Porcelain Transformer Bushings.* Amir S. Gilani, Andrew S. Whittaker, Gregory L. Fenves, and Eric Fujisaki. December 1999.

PEER 1999/13 *Building Vulnerability Studies: Modeling and Evaluation of Tilt-up and Steel Reinforced Concrete Buildings.* John W. Wallace, Jonathan P. Stewart, and Andrew S. Whittaker, editors. December 1999.

PEER 1999/12 *Rehabilitation of Nonductile RC Frame Building Using Encasement Plates and Energy-Dissipating Devices.* Mehrdad Sasani, Vitelmo V. Bertero, James C. Anderson. December 1999.

PEER 1999/11 *Performance Evaluation Database for Concrete Bridge Components and Systems under Simulated Seismic Loads.* Yael D. Hose and Frieder Seible. November 1999.

PEER 1999/10 *U.S.-Japan Workshop on Performance-Based Earthquake Engineering Methodology for Reinforced Concrete Building Structures.* December 1999.

PEER 1999/09 *Performance Improvement of Long Period Building Structures Subjected to Severe Pulse-Type Ground Motions.* James C. Anderson, Vitelmo V. Bertero, and Raul Bertero. October 1999.

PEER 1999/08 *Envelopes for Seismic Response Vectors.* Charles Menun and Armen Der Kiureghian. July 1999.

PEER 1999/07 *Documentation of Strengths and Weaknesses of Current Computer Analysis Methods for Seismic Performance of Reinforced Concrete Members.* William F. Cofer. November 1999.

PEER 1999/06 *Rocking Response and Overturning of Anchored Equipment under Seismic Excitations.* Nicos Makris and Jian Zhang. November 1999.

PEER 1999/05 *Seismic Evaluation of 550 kV Porcelain Transformer Bushings.* Amir S. Gilani, Andrew S. Whittaker, Gregory L. Fenves, and Eric Fujisaki. October 1999.

PEER 1999/04 *Adoption and Enforcement of Earthquake Risk-Reduction Measures.* Peter J. May, Raymond J. Burby, T. Jens Feeley, and Robert Wood.

PEER 1999/03 *Task 3 Characterization of Site Response General Site Categories.* Adrian Rodriguez-Marek, Jonathan D. Bray, and Norman Abrahamson. February 1999.

PEER 1999/02 *Capacity-Demand-Diagram Methods for Estimating Seismic Deformation of Inelastic Structures: SDF Systems.* Anil K. Chopra and Rakesh Goel. April 1999.

PEER 1999/01 *Interaction in Interconnected Electrical Substation Equipment Subjected to Earthquake Ground Motions.* Armen Der Kiureghian, Jerome L. Sackman, and Kee-Jeung Hong. February 1999.

PEER 1998/08 *Behavior and Failure Analysis of a Multiple-Frame Highway Bridge in the 1994 Northridge Earthquake.* Gregory L. Fenves and Michael Ellery. December 1998.

PEER 1998/07 *Empirical Evaluation of Inertial Soil-Structure Interaction Effects.* Jonathan P. Stewart, Raymond B. Seed, and Gregory L. Fenves. November 1998.

PEER 1998/06 *Effect of Damping Mechanisms on the Response of Seismic Isolated Structures.* Nicos Makris and Shih-Po Chang. November 1998.

PEER 1998/05 *Rocking Response and Overturning of Equipment under Horizontal Pulse-Type Motions.* Nicos Makris and Yiannis Roussos. October 1998.

PEER 1998/04 *Pacific Earthquake Engineering Research Invitational Workshop Proceedings, May 14–15, 1998: Defining the Links between Planning, Policy Analysis, Economics and Earthquake Engineering.* Mary Comerio and Peter Gordon. September 1998.

PEER 1998/03 *Repair/Upgrade Procedures for Welded Beam to Column Connections.* James C. Anderson and Xiaojing Duan. May 1998.

PEER 1998/02 *Seismic Evaluation of 196 kV Porcelain Transformer Bushings.* Amir S. Gilani, Juan W. Chavez, Gregory L. Fenves, and Andrew S. Whittaker. May 1998.

PEER 1998/01 *Seismic Performance of Well-Confined Concrete Bridge Columns.* Dawn E. Lehman and Jack P. Moehle. December 2000.

ONLINE PEER REPORTS

The following PEER reports are available by Internet only at http://peer.berkeley.edu/publications/peer_reports_complete.html.

PEER 2012/103 *Performance-Based Seismic Demand Assessment of Concentrically Braced Steel Frame Buildings.* Chui-Hsin Chen and Stephen A. Mahin. December 2012.

PEER 2012/102 *Procedure to Restart an Interrupted Hybrid Simulation: Addendum to PEER Report 2010/103.* Vesna Terzic and Bozidar Stojadinovic. October 2012.

PEER 2012/101 *Mechanics of Fiber Reinforced Bearings.* James M. Kelly and Andrea Calabrese. February 2012.

PEER 2011/107 *Nonlinear Site Response and Seismic Compression at Vertical Array Strongly Shaken by 2007 Niigata-ken Chuetsu-oki Earthquake.* Eric Yee, Jonathan P. Stewart, and Kohji Tokimatsu. December 2011.

PEER 2011/106 *Self Compacting Hybrid Fiber Reinforced Concrete Composites for Bridge Columns.* Pardeep Kumar, Gabriel Jen, William Trono, Marios Panagiotou, and Claudia Ostertag. September 2011.

PEER 2011/105 *Stochastic Dynamic Analysis of Bridges Subjected to Spacially Varying Ground Motions.* Katerina Konakli and Armen Der Kiureghian. August 2011.

PEER 2011/104 *Design and Instrumentation of the 2010 E-Defense Four-Story Reinforced Concrete and Post-Tensioned Concrete Buildings.* Takuya Nagae, Kenichi Tahara, Taizo Matsumori, Hitoshi Shiohara, Toshimi Kabeyasawa, Susumu Kono, Minehiro Nishiyama (Japanese Research Team) and John Wallace, Wassim Ghannoum, Jack Moehle, Richard Sause, Wesley Keller, Zeynep Tuna (U.S. Research Team). June 2011.

PEER 2011/103 *In-Situ Monitoring of the Force Output of Fluid Dampers: Experimental Investigation.* Dimitrios Konstantinidis, James M. Kelly, and Nicos Makris. April 2011.

PEER 2011/102 *Ground-motion prediction equations 1964 - 2010.* John Douglas. April 2011.

PEER 2011/101 *Report of the Eighth Planning Meeting of NEES/E-Defense Collaborative Research on Earthquake Engineering.* Convened by the Hyogo Earthquake Engineering Research Center (NIED), NEES Consortium, Inc. February 2011.

PEER 2010/111 *Modeling and Acceptance Criteria for Seismic Design and Analysis of Tall Buildings.* Task 7 Report for the Tall Buildings Initiative - Published jointly by the Applied Technology Council. October 2010.

PEER 2010/110 *Seismic Performance Assessment and Probabilistic Repair Cost Analysis of Precast Concrete Cladding Systems for Multistory Buildlings.* Jeffrey P. Hunt and Božidar Stojadinovic. November 2010.

PEER 2010/109 *Report of the Seventh Joint Planning Meeting of NEES/E-Defense Collaboration on Earthquake Engineering. Held at the E-Defense, Miki, and Shin-Kobe, Japan, September 18–19, 2009.* August 2010.

PEER 2010/108 *Probabilistic Tsunami Hazard in California.* Hong Kie Thio, Paul Somerville, and Jascha Polet, preparers. October 2010.

PEER 2010/107 *Performance and Reliability of Exposed Column Base Plate Connections for Steel Moment-Resisting Frames.* Ady Aviram, Božidar Stojadinovic, and Armen Der Kiureghian. August 2010.

PEER 2010/106 *Verification of Probabilistic Seismic Hazard Analysis Computer Programs.* Patricia Thomas, Ivan Wong, and Norman Abrahamson. May 2010.

PEER 2010/105 *Structural Engineering Reconnaissance of the April 6, 2009, Abruzzo, Italy, Earthquake, and Lessons Learned.* M. Selim Günay and Khalid M. Mosalam. April 2010.

PEER 2010/104 *Simulating the Inelastic Seismic Behavior of Steel Braced Frames, Including the Effects of Low-Cycle Fatigue.* Yuli Huang and Stephen A. Mahin. April 2010.

PEER 2010/103 *Post-Earthquake Traffic Capacity of Modern Bridges in California.* Vesna Terzic and Božidar Stojadinović. March 2010.

PEER 2010/102 *Analysis of Cumulative Absolute Velocity (CAV) and JMA Instrumental Seismic Intensity (I_{JMA}) Using the PEER–NGA Strong Motion Database.* Kenneth W. Campbell and Yousef Bozorgnia. February 2010.

PEER 2010/101 *Rocking Response of Bridges on Shallow Foundations.* Jose A. Ugalde, Bruce L. Kutter, and Boris Jeremic. April 2010.

PEER 2009/109 *Simulation and Performance-Based Earthquake Engineering Assessment of Self-Centering Post-Tensioned Concrete Bridge Systems.* Won K. Lee and Sarah L. Billington. December 2009.

PEER 2009/108 *PEER Lifelines Geotechnical Virtual Data Center.* J. Carl Stepp, Daniel J. Ponti, Loren L. Turner, Jennifer N. Swift, Sean Devlin, Yang Zhu, Jean Benoit, and John Bobbitt. September 2009.

PEER 2009/107 *Experimental and Computational Evaluation of Current and Innovative In-Span Hinge Details in Reinforced Concrete Box-Girder Bridges: Part 2: Post-Test Analysis and Design Recommendations.* Matias A. Hube and Khalid M. Mosalam. December 2009.

PEER 2009/106 *Shear Strength Models of Exterior Beam-Column Joints without Transverse Reinforcement.* Sangjoon Park and Khalid M. Mosalam. November 2009.

PEER 2009/105 *Reduced Uncertainty of Ground Motion Prediction Equations through Bayesian Variance Analysis.* Robb Eric S. Moss. November 2009.

PEER 2009/104 *Advanced Implementation of Hybrid Simulation.* Andreas H. Schellenberg, Stephen A. Mahin, Gregory L. Fenves. November 2009.

PEER 2009/103 *Performance Evaluation of Innovative Steel Braced Frames.* T. Y. Yang, Jack P. Moehle, and Božidar Stojadinovic. August 2009.

PEER 2009/102 *Reinvestigation of Liquefaction and Nonliquefaction Case Histories from the 1976 Tangshan Earthquake.* Robb Eric Moss, Robert E. Kayen, Liyuan Tong, Songyu Liu, Guojun Cai, and Jiaer Wu. August 2009.

PEER 2009/101 *Report of the First Joint Planning Meeting for the Second Phase of NEES/E-Defense Collaborative Research on Earthquake Engineering.* Stephen A. Mahin et al. July 2009.

PEER 2008/104 *Experimental and Analytical Study of the Seismic Performance of Retaining Structures.* Linda Al Atik and Nicholas Sitar. January 2009.

PEER 2008/103 *Experimental and Computational Evaluation of Current and Innovative In-Span Hinge Details in Reinforced Concrete Box-Girder Bridges. Part 1: Experimental Findings and Pre-Test Analysis.* Matias A. Hube and Khalid M. Mosalam. January 2009.

PEER 2008/102 *Modeling of Unreinforced Masonry Infill Walls Considering In-Plane and Out-of-Plane Interaction.* Stephen Kadysiewski and Khalid M. Mosalam. January 2009.

PEER 2008/101 *Seismic Performance Objectives for Tall Buildings.* William T. Holmes, Charles Kircher, William Petak, and Nabih Youssef. August 2008.

PEER 2007/101 *Generalized Hybrid Simulation Framework for Structural Systems Subjected to Seismic Loading.* Tarek Elkhoraibi and Khalid M. Mosalam. July 2007.

PEER 2007/100 *Seismic Evaluation of Reinforced Concrete Buildings Including Effects of Masonry Infill Walls.* Alidad Hashemi and Khalid M. Mosalam. July 2007.

The Pacific Earthquake Engineering Research Center (PEER) is a multi-institutional research and education center with headquarters at the University of California, Berkeley. Investigators from over 20 universities, several consulting companies, and researchers at various state and federal government agencies contribute to research programs focused on performance-based earthquake engineering.

These research programs aim to identify and reduce the risks from major earthquakes to life safety and to the economy by including research in a wide variety of disciplines including structural and geotechnical engineering, geology/seismology, lifelines, transportation, architecture, economics, risk management, and public policy.

PEER is supported by federal, state, local, and regional agencies, together with industry partners.

PEER Core Institutions:
University of California, Berkeley (Lead Institution)
California Institute of Technology
Oregon State University
Stanford University
University of California, Davis
University of California, Irvine
University of California, Los Angeles
University of California, San Diego
University of Southern California
University of Washington

PEER reports can be ordered at http://peer.berkeley.edu/publications/peer_reports.html or by contacting

Pacific Earthquake Engineering Research Center
University of California, Berkeley
325 Davis Hall, mail code 1792
Berkeley, CA 94720-1792
Tel: 510-642-3437
Fax: 510-642-1655
Email: peer_editor@berkeley.edu

ISSN 1547-0587X